

Article

Towards Optimized Photoluminescent Copper(I) Phenanthroline-Functionalized Complexes: Control of the Photophysics by Symmetry-Breaking and Spin–Orbit Coupling

Christophe Gourlaouen * and Chantal Daniel 

Laboratoire de Chimie Quantique Institut de Chimie UMR 7177, CNRS, Université de Strasbourg, 4, Rue Blaise Pascal CS 90032, F-67081 Strasbourg, France; c.daniel@unistra.fr

* Correspondence: gourlaouen@unistra.fr

Abstract: The electronic and structural alterations induced by the functionalization of the 1,10-phenanthroline (phen) ligand in [Cu(I) (phen- R_2) $_2$] $^+$ complexes ($R=H, CH_3, tertio$ -butyl, alkyl-linkers) and their consequences on the luminescence properties and thermally activated delay fluorescence (TADF) activity are investigated using the density functional theory (DFT) and its time-dependent (TD) extension. It is shown that highly symmetric molecules with several potentially emissive nearly-degenerate conformers are not promising because of low S_1/S_0 oscillator strengths together with limited or no S_1/T_1 spin–orbit coupling (SOC). Furthermore, steric hindrance, which prevents the flattening of the complex upon irradiation, is a factor of instability. Alternatively, linking the phenanthroline ligands offers the possibility to block the flattening while maintaining remarkable photophysical properties. We propose here two promising complexes, with appropriate symmetry and enough rigidity to warrant stability in standard solvents. This original study paves the way for the supramolecular design of new emissive devices.



Citation: Gourlaouen, C.; Daniel, C.

Towards Optimized Photoluminescent Copper(I) Phenanthroline-Functionalized Complexes: Control of the Photophysics by Symmetry-Breaking and Spin–Orbit Coupling. *Materials* **2022**, *15*, 5222. <https://doi.org/10.3390/ma15155222>

Academic Editor: Dong-Joo Kim

Received: 22 June 2022

Accepted: 21 July 2022

Published: 28 July 2022

Publisher's Note: MDPI stays neutral with regard to jurisdictional claims in published maps and institutional affiliations.



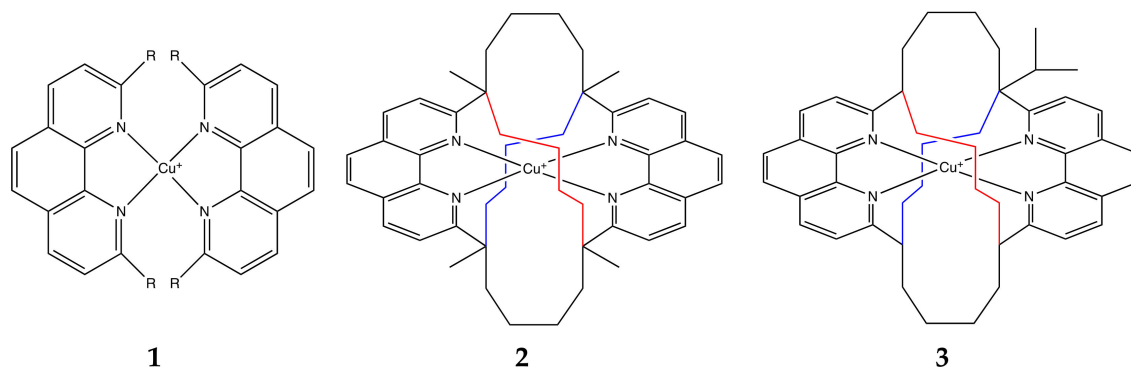
Copyright: © 2022 by the authors. Licensee MDPI, Basel, Switzerland. This article is an open access article distributed under the terms and conditions of the Creative Commons Attribution (CC BY) license (<https://creativecommons.org/licenses/by/4.0/>).

Keywords: luminescence; TADF; copper(I) phenanthroline functionalization; density functional theory; nuclear relaxation; symmetry-breaking spin–orbit coupling

1. Introduction

The emissive properties of bis-phenanthroline substituted Cu(I) complexes have been intensively explored starting in the late 70s [1–4] because of intriguing luminescence properties extremely sensitive to structural effects driven by the surrounding ligands [5–26]. The development of time-resolved spectroscopies and pump–probe X-ray experiments has allowed the mapping of ultrafast kinetics that precede the formation of potentially long-lived triplet T_1 excited states [26–43]. The decay mechanism involves several intermediate singlet and triplet excited states coupled vibronically and by spin–orbit [44–49], the influence of the solvent being significant on the emission properties [50,51]. The relationship between the observed structural distortions, triggered by visible irradiation, and the excited state dynamics is not clear enough for a rigorous rationalization of the luminescent behavior of a variety of more or less constrained complexes proposed over the years. The structural reorganization in the active metal-to-ligand charge transfer (MLCT) state, from the pseudo tetrahedral D_{2d} symmetry ground state to a flattened D_2 symmetry excited state, has been investigated combining various spectroscopies with the functionalization of the phenanthrolines [31,33,39,40,52–54] (thereafter phen). The hope is to inhibit, by steric hindrance, the early pseudo-Jahn–Teller (PJT) distortion induced by the MLCT electronic transition and to prevent the formation of the flattened structure, critical to generate the appropriate long-lived 3MLCT state and high photoluminescence quantum yields. However, the synthesis of stable complexes with bulky ligands is still a challenge and the resulting photophysical properties do not always live up to expectations [55–58].

The present theoretical study is dedicated to a comparative investigation of the structural, optical and emissive properties of five [Cu(I) (phen-R₂)₂]⁺ complexes (R=H (**1_H**), CH₃ (**1_{Me}**), *tertio*-butyl (**1_{tBu}**) and alkyl-linker (**2** and **3**), Scheme 1) of increasing steric complexity associated with symmetry breaking. The potential energy profiles associated with the low-lying singlet and triplet excited states as well as their spin–orbit coupling (SOC) as a function of the structural deformations are scrutinized in order to rationalize the photophysical behavior within the series and to point to the consequence of symmetry-breaking on emission properties. In contrast to previous theoretical studies, the implication of upper triplet states and advanced spin–orbit effects are considered going beyond an oversimplified S₁/T₁ two-state model based on frontier molecular orbitals.



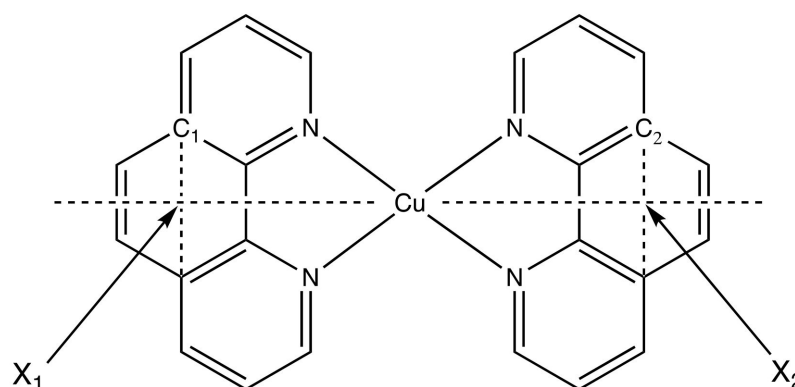
Scheme 1. Schematic structures of complexes **1** (R=H, **1_H**; CH₃, **1_{Me}**; *tertio*-butyl, **1_{tBu}**) **2** and **3**.

2. Computational Method

A first set of calculations has been performed with GAUSSIAN 09 (version D01) [59] at a density functional theory (DFT) level of theory with B3LYP functional [60] in CH₂Cl₂ through a PCM model [61]. All atoms were described by Pople's 6-31+G** basis set [62]. Structures in the ground state and in triplet states were fully optimized and the nature of the encountered stationary point was checked by frequency analysis. Minima were characterized by a full set of real frequencies and the transition state by one imaginary frequency. Dispersion corrections were introduced through Grimme's corrections [63].

A second set of calculations was performed with the ADF 2019 package [64]. The complexes (Scheme 1) electronic ground state and low-lying excited singlet and triplet state structures have been optimized by means of DFT using the B3LYP functional [60] and triple- ζ basis sets for all atoms [65]. Scalar relativistic effects were included using zeroth-order relativistic Hamiltonian [66]. Grimme's corrections have been applied to consider dispersion effects [67]. Calculations have been performed in CH₂Cl₂ within the COSMO (conductor-like screening model) approximation [68]. The absorption spectra were computed at the TD-DFT level, including perturbative spin–orbit effects [69,70]. The Tamm–Dancoff approximation (TDA) was employed in order to avoid triplet instability problems [71].

Cuts of the potential energy surfaces along the key nuclear coordinates (Scheme 2), namely the Cu–phen distance (Cu–X₁), the rocking angle (X₁–Cu–X₂) and the dihedral flattening angle (C₁–X₁–X₂–C₂), were obtained with remaining coordinates frozen at the ground state structure with ADF.



Scheme 2. Schematic view of the molecules with the key nuclear coordinates, with X_1 and X_2 being the center of the phenyl core.

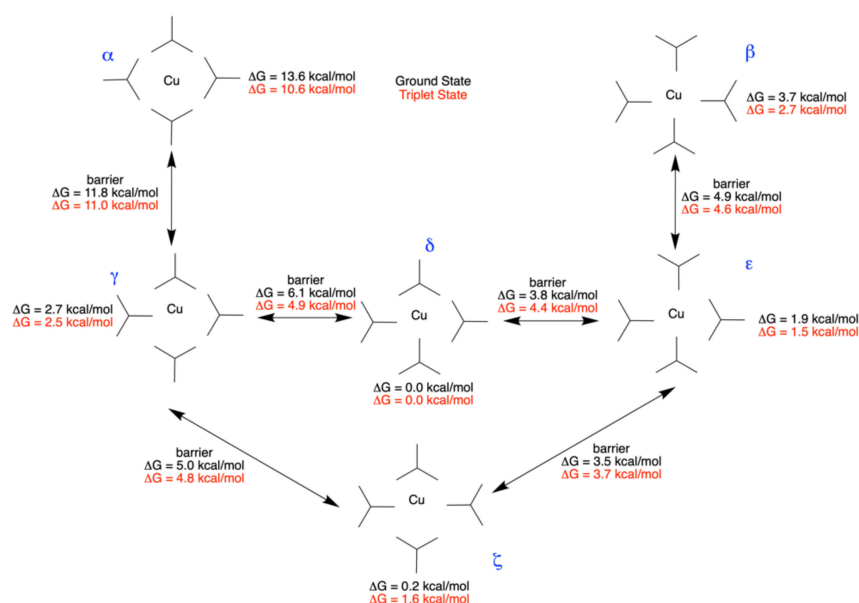
The excited state analysis was performed by TheoDORE, a package for theoretical density, orbital relaxation and exciton analysis [72].

3. Results

3.1. Ground State and Excited State Structural Properties

The structural data, namely a fully optimized electronic ground state and lowest T_1 excited state optimized with GAUSSIAN are given in the SI section. The complexes are structurally flexible even in the ground state (GS) due to the weak inter-ligand interactions. This is illustrated by the variety of 1_H GS crystal structures [73–80] (Table S1 in Supplementary Materials), for which the structural parameters depend on the nature of the counter-anion and of the solvent in which the compounds were crystallized. The Cu–N distances vary from 1.996 Å to 2.081 Å, the X_1 –Cu– X_2 angle from 144.8° to 180.0° and the C_1 – X_1 – X_2 – C_2 dihedral from 33.9° to 90° (Table S1). The situation is similar for 1_{Me} [81–86] (Table S2). In both cases, the computed GS structure is within the range of experimental data. The situation is different for 1_{tBu} , the bulkiness of the tertio-butyl group prevents the significant distortion of the geometry. However, this group introduces a new degree of freedom in the structure according to the orientation of the tertio-butyl groups. For each of them, there are two possibilities, a methyl group can point towards the copper cation or to the opposite of the cation (Figure S1). This generates six possible conformers (Scheme 3, Table S3), four of them (γ , δ , ϵ , ζ) exhibiting energy differences lower than 3 kcal mol^{−1} and separated by barriers lower than 7 kcal mol^{−1}. This implies that in the solution there is a thermal distribution of the conformers in fast equilibrium. This is supported by the experimental structures of 1_{tBu} [87]. Depending on the complex environment, the structure can adopt different conformations in the crystal (Table S4). According to frequency analysis, the GS structures of 1_H and 1_{Me} are of D_{2d} symmetry point group, that of 1_{tBu} most stable conformer (δ) is only C_2 . **2** exhibits C_{2v} symmetry and **3** has C_s symmetry (Table S3).

The structural evolution is complex during excited state relaxation. In the optimized structures of the T_1 excited state of 1_H and 1_{Me} , a significant flattening of the complex is observed leading to a D_2 symmetry structure. The C_1 – X_1 – X_2 – C_2 angle falls to 41.5° for 1_H and to 65° for 1_{Me} (Table S5). In contrast, for 1_{tBu} (steric constraints, Table S5), **2** and **3** (ligand rigidity, Table S5), there is almost no flattening. The flattening generates two degenerated minima in 1_H and 1_{Me} , depending on the rotational direction (Scheme S1). These two structures are connected by a transition state (thereafter TS1) of 12.9 kcal mol^{−1} for 1_H and 4.4 kcal mol^{−1} for 1_{Me} .



Scheme 3. Schematic structure (only the tBu groups are represented), name and energies computed with a GAUSSIAN of the different conformers of 1_{tBu} in the ground state (black values) and in the lowest triplet state (red values).

The symmetry of 1_{Me} and 1_{tBu} is also reduced by the Cu–N bond breathing. One phen ligand is associated with a significant shortening of the Cu–N bonds, between 0.05 and 0.20 Å. The relaxation of the second phen ligand depends on the steric hindrance with a Cu–N bond shortening in 1_{Me} (Table S5) and a lengthening in 1_{tBu} (Table S5). A similar distortion operates in complexes **2** and **3**. The bond breathing generates for each complex (except for 1_H) two minima in T1 connected by a transition state (thereafter TS2). These minima are strictly degenerate for 1_{Me} and 1_{tBu} , the two phen being identical in these molecules. In **2** and **3**, the linkers induce constraints on the phen ligands and slightly lift the degeneracy of the two minima. The barrier associated with TS2 is very low, 2.4 kcal mol^{−1} for 1_{tBu} . The flattening induces two minima depending on the phen orientations (left and right) in 1_H and 1_{Me} . Consequently, the T1 PES is characterized by four minima in 1_{Me} (breathing and flattening, Scheme S1), two minima in 1_H (flattening), two minima in **2** and **3** (breathing). The case of 1_{tBu} is more complicated. The orientation of the tBu groups generates six possible conformers in the ground state (Scheme 3), number potentially doubled in the T1 excited state due to the bond breathing. Though some conformers (α , β) can be neglected due to their relative instability, the others may play a central role in the luminescence properties. More specifically, the most stable δ conformer (Scheme 3) will be used as reference for the 1_{tBu} excited state properties described below.

The calculated values of TS1 and TS2 are in favor of non-negligible dynamical effects. The bond breathing (TS2) is associated with low barriers and the occurrence of true minima is uncertain. Furthermore, the barriers increase with the steric hindrance of the R group (none for 1_H , and $1_{Me} < 1_{tBu}$). The formal oxidation of the copper tends to shorten the Cu–N bonds. However, the ligand repulsion in T1 counterbalances this shortening leading to a pendulum motion: one ligand approaches the copper while the second one moves away from it. This effect increases with the size of the R group. The movement of interconversion of the phen (TS1) is more costly but possible for 1_{Me} at the time-scale of excited state lifetime.

3.2. Low-Lying Singlet and Triplet Excited State Properties

3.2.1. Energetics, Absorption Spectra and Spin–Orbit Coupling

The calculated absorption spectra are depicted in Figure 1 on the basis of ADF optimized structure. The transition energies, absorption wavelengths and oscillator strengths associated with the 25 lowest singlet excited states of complexes 1_H , 1_{Me} , 1_{tBu} , **2** and **3** are

reported in Tables 1 and 2, respectively. Complexes **1** absorb in the visible at ~490 nm via the 3rd singlet excited state (S3, $f > 10^{-1}$) and in the UV domain ($f > 10^{-2}$) at ~340 nm (S17) and at ~320 nm (S23). The orientation of the tBu groups does not affect the structure of the absorption spectrum of **1**_{tBu}, inducing insignificant shifts of about 25 nm in the position of the absorption bands (Figure S2).

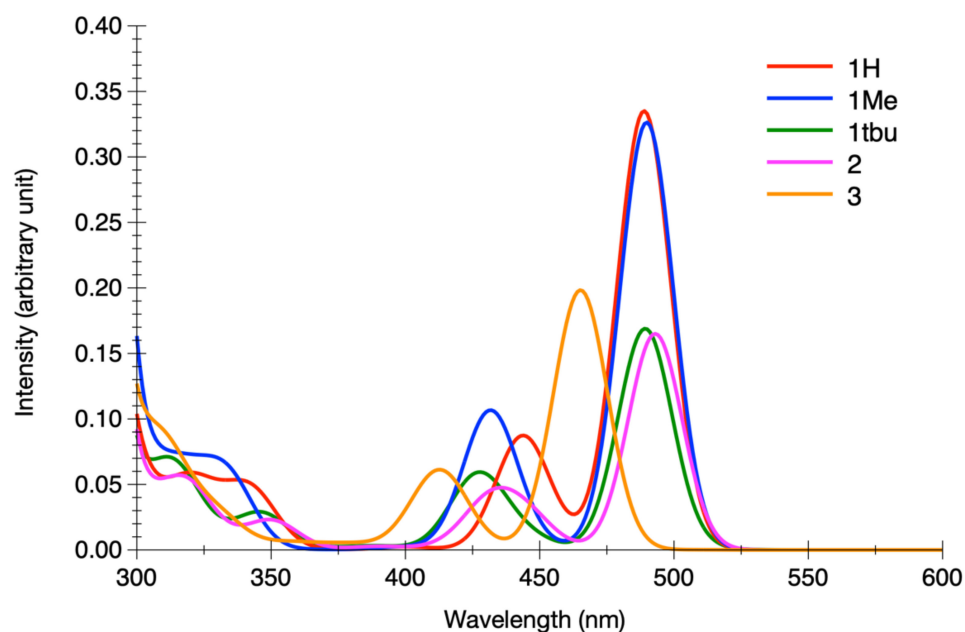


Figure 1. Calculated TD-DFT absorption spectra without spin-orbit.

Table 1. S0 to S_n transition energies (ADF) E^{abs} (eV), absorption wavelengths λ^{abs} (in nm) and oscillator strengths (f) of [Cu(I) (phen-R₂)₂]⁺ complexes **1** (**1**_H, **1**_{Me}, and δ conformation of **1**_{tBu}).

State	1 _H			1 _{Me}			1 _{tBu} (δ)		
	E^{abs}	λ^{abs}	f	E^{abs}	λ^{abs}	f	E^{abs}	λ^{abs}	f
S1	2.370	523	7.91×10^{-13}	2.361	525	1.17×10^{-13}	2.419	513	1.30×10^{-3}
S2	2.427	511	5.49×10^{-11}	2.421	512	2.71×10^{-11}	2.465	503	9.46×10^{-5}
S3	2.536	489	3.35×10^{-1}	2.531	490	3.26×10^{-1}	2.534	489	1.69×10^{-1}
S4	2.699	459	8.94×10^{-4}	2.775	447	2.20×10^{-3}	2.778	446	7.14×10^{-3}
S5	2.699	459	8.77×10^{-4}	2.790	444	2.31×10^{-3}	2.810	441	2.34×10^{-3}
S6	2.789	445	4.48×10^{-2}	2.873	431	5.25×10^{-2}	2.864	433	3.91×10^{-3}
S7	2.800	443	4.24×10^{-2}	2.873	431	5.25×10^{-2}	2.895	428	3.24×10^{-2}
S8	3.031	409	2.21×10^{-6}	3.029	409	1.54×10^{-6}	2.912	426	1.40×10^{-2}
S9	3.101	400	1.19×10^{-3}	3.101	400	1.16×10^{-3}	2.915	425	2.67×10^{-3}
S10	3.101	400	1.20×10^{-3}	3.121	397	1.16×10^{-3}	2.948	421	6.70×10^{-3}
S11	3.265	380	2.96×10^{-5}	3.287	377	6.67×10^{-5}	3.157	393	9.42×10^{-6}
S12	3.276	378	2.68×10^{-5}	3.298	376	6.74×10^{-5}	3.170	391	1.82×10^{-3}
S13	3.379	367	1.27×10^{-4}	3.401	365	1.26×10^{-4}	3.212	386	6.36×10^{-4}
S14	3.379	367	1.26×10^{-4}	3.401	365	1.37×10^{-4}	3.213	386	6.01×10^{-4}
S15	3.454	359	1.51×10^{-14}	3.526	352	7.98×10^{-13}	3.329	372	3.68×10^{-4}
S16	3.462	358	3.21×10^{-12}	3.554	349	6.72×10^{-13}	3.342	371	7.34×10^{-4}
S17	3.628	342	4.70×10^{-2}	3.722	333	5.69×10^{-2}	3.581	346	2.71×10^{-2}

Table 1. Cont.

State	1_H			1_{Me}			$1_{tBu} (\delta)$		
	E^{abs}	λ^{abs}	f	E^{abs}	λ^{abs}	f	E^{abs}	λ^{abs}	f
S18	3.680	337	9.90×10^{-7}	3.793	327	1.12×10^{-6}	3.624	342	4.93×10^{-4}
S19	3.753	330	4.65×10^{-9}	3.829	324	3.72×10^{-11}	3.625	342	1.04×10^{-3}
S20	3.771	329	2.53×10^{-14}	3.857	321	3.58×10^{-13}	3.642	340	4.41×10^{-5}
S21	3.812	325	1.14×10^{-12}	3.895	318	2.63×10^{-13}	3.841	323	2.03×10^{-3}
S22	3.818	325	1.38×10^{-9}	3.895	318	1.03×10^{-10}	3.861	321	1.26×10^{-5}
S23	3.875	320	4.99×10^{-2}	3.929	316	4.04×10^{-2}	3.917	317	3.12×10^{-2}
S24	4.012	309	3.19×10^{-7}	3.958	313	1.53×10^{-7}	3.966	313	3.84×10^{-3}
S25	4.079	304	1.48×10^{-2}	4.027	308	2.27×10^{-2}	4.009	309	3.50×10^{-2}

Table 2. S0 to Sn transition energies (ADF) E^{abs} (eV), absorption wavelengths λ^{abs} (in nm) and oscillator strengths (f) of $[Cu(I) (\text{phen-R}_2)_2]^+$ complexes 2 and 3.

State	2			3		
	E^{abs}	λ^{abs}	f	E^{abs}	λ^{abs}	f
S1	2.381	521	1.63×10^{-6}	2.448	506	1.69×10^{-4}
S2	2.434	509	3.08×10^{-6}	2.659	466	6.74×10^{-2}
S3	2.515	493	1.65×10^{-1}	2.669	465	1.32×10^{-1}
S4	2.730	454	2.20×10^{-4}	2.848	435	6.53×10^{-4}
S5	2.767	448	9.72×10^{-5}	2.968	418	9.83×10^{-3}
S6	2.782	446	2.33×10^{-2}	2.990	415	2.31×10^{-2}
S7	2.856	434	6.03×10^{-3}	3.013	411	7.92×10^{-3}
S8	2.877	431	3.02×10^{-2}	3.029	409	2.31×10^{-2}
S9	2.886	430	2.08×10^{-4}	3.125	397	1.21×10^{-3}
S10	2.994	414	2.01×10^{-3}	3.230	384	1.92×10^{-3}
S11	3.093	401	1.99×10^{-4}	3.297	376	3.07×10^{-3}
S12	3.116	398	1.25×10^{-5}	3.320	373	1.98×10^{-5}
S13	3.174	391	1.66×10^{-3}	3.439	360	8.82×10^{-4}
S14	3.212	386	1.03×10^{-3}	3.469	357	3.24×10^{-3}
S15	3.299	376	2.67×10^{-6}	3.501	354	1.62×10^{-3}
S16	3.338	371	1.75×10^{-7}	3.605	344	1.83×10^{-4}
S17	3.515	353	1.08×10^{-6}	3.728	333	6.97×10^{-4}
S18	3.544	350	2.26×10^{-2}	3.759	330	2.34×10^{-2}
S19	3.551	349	2.97×10^{-7}	3.826	324	2.27×10^{-5}
S20	3.618	343	2.38×10^{-4}	3.844	323	2.48×10^{-3}
S21	3.705	335	6.04×10^{-7}	3.904	318	1.04×10^{-4}
S22	3.879	320	3.74×10^{-2}	3.936	315	5.64×10^{-3}
S23	3.892	319	8.98×10^{-6}	3.962	313	3.21×10^{-4}
S24	3.930	315	7.24×10^{-3}	3.992	311	1.78×10^{-2}
S25	3.993	310	1.31×10^{-2}	4.029	308	5.14×10^{-2}

The absorption properties of complex **2** are very similar with three bands at 493 nm (S3), 350 (S18) and 320 nm (S22). The absorption of complex **3** starts at 465 nm (S3, $f > 10^{-1}$), slightly blue-shifted as compared to the other complexes. As illustrated in Figure 2, the low-lying singlet excited states of the five complexes are mainly of metal-to-ligand charge transfer (MLCT) character with minor additions of ligand-centered (LC) and ligand-to-ligand charge transfer (LLCT). These states principally arise from HOMO and HOMO-1 orbitals towards LUMO to LUMO+3 (Figures S3 and S4).

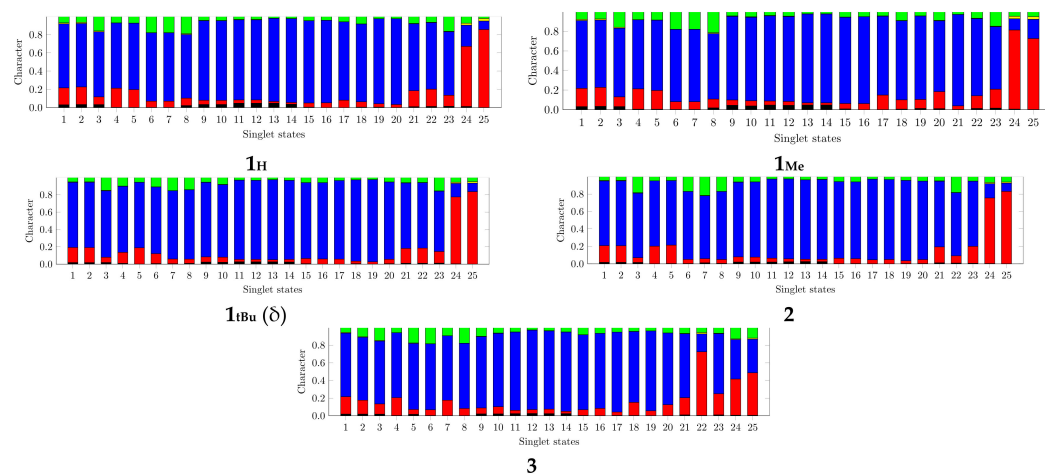


Figure 2. TheoDOR analysis of the lowest absorbing singlet states of complexes **1H**, **1Me**, **1tBu(δ)**, **2** and **3**. In black are metal-centered transitions; in red, ligand-centered transitions; in blue, metal-to-ligand charge transfer; in yellow, ligand-to-metal charge transfer and in green, ligand-to-ligand charge transfer. The state numbers corresponding to main transitions (Tables 1 and 2) are in bold.

From TheoDOR analysis (Figure 3), it appears that the low-lying triplet states are essentially MLCT with increasing LC contributions when moving to higher excitation energies. Including spin-orbit corrections does not modify the absorption spectra because the low-lying triplet states do not gain intensity by SOC, as illustrated by the data reported in Tables 3 and 4, which describe the transition energies of the “spin-orbit” states together with associated oscillator strengths and state mixing. Table 5 reports spin-orbit mixing between the low-lying singlet and triplet states.

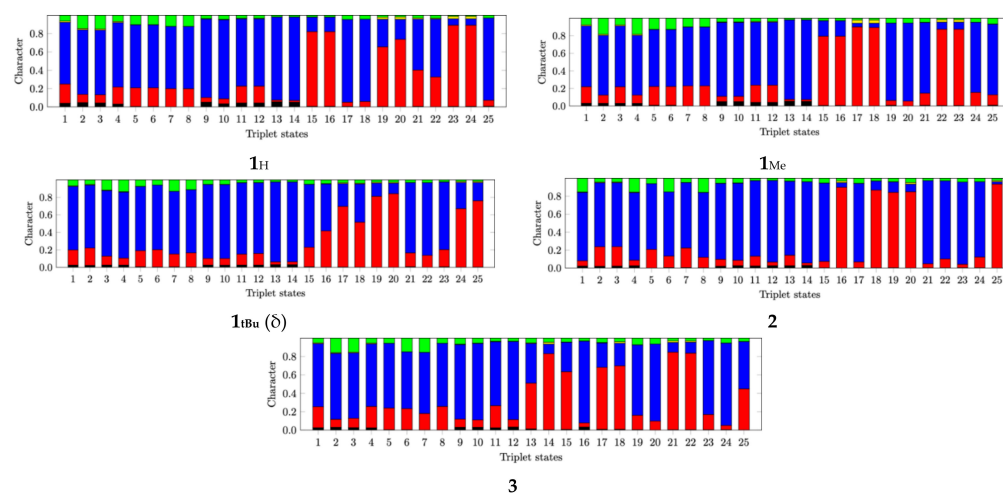


Figure 3. TheoDOR analysis of the lowest triplet states at Franck-Condon geometry of complexes **1H**, **1Me**, **1tBu(δ)**, **2** and **3**. In black are metal-centered transitions; in red, ligand-centered transitions; in blue, metal-to-ligand charge transfer; in yellow, ligand-to-metal charge transfer and in green, ligand-to-ligand charge transfer.

Table 3. Spin–orbit excited states: transition energies (in eV), oscillator strengths, mixing in terms of Sn/Tn states of complexes **1_H**, **1_{Me}**, **1_{tBu}** (δ).

State	1_H			1_{Me}			1_{tBu}		
	E^{abs}	f	Mixing	E^{abs}	f	Mixing	E^{abs}	f	Mixing
E1	2.241	4.16×10^{-6}	T1 83% T4 16%	2.233	6.36×10^{-6}	T1 81% T4 18%	2.262	3.35×10^{-6}	T1 85% T4 9% T2 4%
E2	2.241	4.26×10^{-6}	T1 83% T4 16%	2.233	6.31×10^{-6}	T1 81% T4 18%	2.263	2.38×10^{-5}	T1 85% T4 9% T2 4%
E3	2.248	3.26×10^{-6}	T2 61% T3 38%	2.235	4.81×10^{-6}	T2 68% T3 31%	2.269	3.09×10^{-3}	T1 95% S3 2%
E4	2.248	3.29×10^{-6}	T2 61% T3 38%	2.235	4.79×10^{-6}	T2 68% T3 31%	2.290	1.30×10^{-5}	T2 65% T3 28%
E5	2.251	5.76×10^{-3}	T1 97% S3 2%	2.243	5.29×10^{-3}	T1 98% S3 2%	2.291	4.80×10^{-5}	T2 65% T3 29% T1 3%
E6	2.265	1.56×10^{-8}	T2 89% S1 10%	2.249	1.29×10^{-9}	T2 91% S1 9%	2.310	2.11×10^{-5}	T2 98%
E7	2.292	3.43×10^{-7}	T3 99%	2.286	2.29×10^{-9}	T3 99%	2.331	1.17×10^{-3}	T3 82% S1 16%
E8	2.303	1.35×10^{-11}	T4 90% S2 9%	2.289	1.09×10^{-11}	T4 92% S2 8%	2.352	1.25×10^{-5}	T4 86% S2 12%
E9	2.322	6.05×10^{-7}	T3 61% T2 38%	2.311	5.98×10^{-7}	T3 68% T2 31%	2.368	1.09×10^{-5}	T3 55% T2 27% T4 13% T1 3%
E10	2.322	6.37×10^{-7}	T3 61% T2 38%	2.311	6.40×10^{-7}	T3 68% T2 31%	2.368	1.13×10^{-5}	T3 58% T2 27% T4 5% T1 3%
E11	2.329	1.81×10^{-6}	T4 82% T1 16%	2.315	2.18×10^{-6}	T4 80% T1 18%	2.380	9.55×10^{-6}	T4 77% T3 11% T1 8% T2 2%
E12	2.329	1.84×10^{-6}	T4 82% T1 16%	2.315	2.24×10^{-6}	T4 80% T1 18%	2.381	1.57×10^{-5}	T4 75% T3 13% T1 7% T2 3%
E13	2.372	5.45×10^{-8}	S1 89% T2 10%	2.361	3.09×10^{-11}	S1 90% T2 9%	2.422	1.18×10^{-3}	S1 81% T3 15% T14 1%
E14	2.428	5.05×10^{-11}	S2 90% T4 9%	2.421	6.16×10^{-11}	S2 91% T4 7%	2.465	8.10×10^{-5}	S2 85% T4 12% T13 1%
E15	2.529	3.23×10^{-1}	S3 97% T1 2%	2.524	3.15×10^{-1}	S3 97% T1 2%	2.523	1.60×10^{-1}	S3 95% T1 2%
E16	2.617	5.87×10^{-6}	T5 71% T7 26%	2.659	5.21×10^{-9}	T5 49% T6 49%	2.718	6.82×10^{-6}	T5 72% T7 15% T6 9%
E17	2.617	1.06×10^{-4}	T5 71% T7 26%	2.659	1.41×10^{-11}	T5 49% T6 49%	2.718	8.35×10^{-6}	T5 72% T7 16% T6 9%

Table 3. Cont.

State	1_H			1_{Me}			1_{tBu}		
	E^{abs}	<i>f</i>	Mixing	E^{abs}	<i>f</i>	Mixing	E^{abs}	<i>f</i>	Mixing
E18	2.624	5.84×10^{-4}	T5 80% S4 11% T6 4% S5 4%	2.679	4.66×10^{-4}	T6 81% S4 10% T5 8%	2.728	1.46×10^{-3}	T5 90% S7 4% S5 3%
E19	2.637	1.43×10^{-7}	T6 70% T8 25% T7 3%	2.680	4.43×10^{-4}	T5 83% T6 10% S5 8%	2.736	9.80×10^{-6}	T6 68% T8 20% T5 6% T7 4%
E20	2.637	1.46×10^{-4}	T6 70% T8 25% T7 3%	2.700	1.40×10^{-11}	T7 35% T8 35% T6 14% T5 14%	2.736	2.76×10^{-4}	T6 68% T8 20% T7 5% T5 5%

Table 4. Spin-orbit excited states: transition energies (in eV), oscillator strengths, mixing in terms of Sn/Tn states of complexes 2 and 3.

State	2			3		
	E^{abs}	<i>f</i>	Mixing	E^{abs}	<i>f</i>	Mixing
E1	2.223	1.26×10^{-6}	T1 56% T2 38% T3 3%	2.290	2.03×10^{-6}	T1 92% T2 5%
E2	2.223	2.24×10^{-5}	T1 56% T2 38% T3 3%	2.290	1.07×10^{-5}	T1 92% T2 6%
E3	2.243	1.26×10^{-7}	T1 92% S1 6%	2.297	8.58×10^{-4}	T1 98%
E4	2.256	3.29×10^{-3}	T2 97% S3 2%	2.393	8.39×10^{-5}	T2 47% S1 41% T2 10%
E5	2.270	2.80×10^{-6}	T3 60% T2 27% T4 6% T1 6%	2.427	2.14×10^{-6}	T2 82% T4 6% T1 4% T3 4%
E6	2.270	1.25×10^{-5}	T3 59% T2 28% T4 6% T1 6%	2.428	4.79×10^{-5}	T2 80% T3 6% T4 5% T1 5%
E7	2.283	2.17×10^{-4}	T3 98%	2.458	2.19×10^{-3}	T3 44% S1 26% T2 26%
E8	2.297	1.90×10^{-6}	T1 35% T2 31% T3 29% T12 1%	2.461	2.37×10^{-5}	T3 71% T4 16% T2 9%
E9	2.298	4.42×10^{-6}	T1 36% T2 32% T3 29% T12 1%	2.462	4.17×10^{-5}	T3 71% T4 16% T2 10%

Table 4. Cont.

State	2			3		
	E ^{abs}	f	Mixing	E ^{abs}	f	Mixing
E10	2.363	1.25×10^{-6}	S1 50% T4 33% S2 13% T1 2%	2.477	1.66×10^{-3}	T3 50% S1 31% T2 15% S2 1%
E11	2.390	1.41×10^{-6}	S1 41% T4 29% S2 24% T1 4%	2.514	2.32×10^{-3}	T4 96% S2 1%
E12	2.412	1.48×10^{-6}	T4 91% T3 6% T14 2%	2.539	9.12×10^{-7}	T4 75% T3 20%
E13	2.413	2.54×10^{-5}	T4 91% T3 6% S13 1%	2.540	1.16×10^{-5}	T4 75% T3 21%
E14	2.447	1.91×10^{-6}	S2 60% T4 36% T14 2%	2.653	6.59×10^{-2}	S2 90% S3 4%
E15	2.503	1.56×10^{-1}	S3 95% T2 2%	2.662	1.22×10^{-1}	S3 91% S2 4%
E16	2.666	1.56×10^{-4}	T5 74% T7 15% T6 6% T8 4%	2.764	1.29×10^{-4}	T5 87% T6 11%
E17	2.666	2.11×10^{-8}	T5 73% T7 15% T6 6% T8 4%	2.764	7.16×10^{-6}	T5 87% T6 11%
E18	2.671	5.13×10^{-4}	T5 88% S5 6% T6 3% S8 2%	2.771	6.64×10^{-4}	T5 96% S6 3%
E19	2.681	9.91×10^{-6}	T6 57% T7 22% T5 15% T8 5%	2.813	4.31×10^{-4}	S4 66% T6 33%
E20	2.681	1.34×10^{-8}	T6 57% T7 22% T5 15% T8 5%	2.875	1.62×10^{-4}	T6 86% T5 12%

Table 5. Spin–orbit coupling (in cm^{-1}) between the low-lying excited states in $\mathbf{1}_H$, $\mathbf{1}_{tBu}$ (δ), $\mathbf{2}$ and $\mathbf{3}$.

$\mathbf{1}_H$	S1	S2	S3	S4	T1	T2	T3	T4
T1	0.0	0.0	307.4	3.0	0.0	0.0	0.0	390.4
T2	275.7	0.0	0.0	17.3	0.0	0.0	428.6	0.0
T3	0.0	0.0	0.0	11.2	0.0	428.6	0.0	0.0
T4	0.0	300.0	0.0	9.6	390.4	0.0	0.0	0.0
$\mathbf{1}_{tBu}$	S1	S2	S3	S4	T1	T2	T3	T4
T1	114.9	0.5	298.4	21.3	0.0	107.1	1.1	423.7
T2	1.3	57.9	0.8	171.1	107.1	0.0	441.5	2.2
T3	289.2	3.1	118.5	58.9	1.1	441.5	0.0	88.3
T4	0.8	322.4	4.1	25.1	423.7	2.2	88.3	0.0
$\mathbf{2}$	S1	S2	S3	S4	T1	T2	T3	T4
T1	282.2	139.9	0.2	7.0	0.0	392.7	201.9	0.4
T2	0.3	0.4	302.1	5.6	392.7	0.0	0.5	183.7
T3	0.1	302.1	76.5	9.9	201.9	0.5	0.0	399.3
T4	129.8	5.6	0.5	22.4	0.4	183.7	399.3	0.0
$\mathbf{3}$	S1	S2	S3	S4	T1	T2	T3	T4
T1	7.9	159.0	221.6	20.5	0.0	425.3	176.5	21.4
T2	316.8	65.3	48.9	23.0	425.3	0.0	24.8	206.9
T3	97.4	248.0	210.6	5.4	176.5	24.8	0.0	411.0
T4	8.6	149.2	124.8	10.2	21.4	206.9	411.0	0.0

Whereas SOC has no effect on the absorption process, we may expect a large influence of SO effects on the early time photophysics. Indeed, within 0.28 eV, we find three singlet (S3, S2, S1) and four triplet (T4, T3, T2, T1) states, all MLCT and potentially activated by absorption, vibronic and spin–orbit coupling for driving the ultrafast decay observed experimentally [38] and tentatively analyzed by quantum dynamics simulations [45] for complex $\mathbf{1}_H$. These seven states, significantly coupled by SOC, lead to a high density of spin–orbit states for all complexes (Tables 3 and 4) between 2.24 eV (E1) and 2.53 eV (E15) in favor of an ultrafast S3 to T1 decay via an efficient spin–vibronic mechanism induced at Franck–Condon by Cu–N breathing mode activation within ~ 100 fs and at a longer time-scale (~ 400 fs) by the PJT distortion, in the case of D_{2d} complexes $\mathbf{1}_H$ and $\mathbf{1}_{Me}$ [44,48–50]. In the highly symmetric molecules, singlets S3, S2 and S1 are strongly coupled with triplet T1, T4 and T2, respectively; T4 and T3 being strongly coupled to T1 and T2, respectively (Table 5). Breaking the symmetry in the sterically-hindered complex $\mathbf{1}_{tBu}$, complexes $\mathbf{2}$ and $\mathbf{3}$ do not drastically modify the energetics but influence the SO interactions, potentially increasing the singlet–triplet interactions at Franck–Condon, in particular S1/T1 and S3/T3 (complex $\mathbf{1}_{tBu}$; complex $\mathbf{2}$) or S2/T1, S3/T2, S3/T3 and T2/T1 in complex $\mathbf{3}$. However, inhibiting the PJT distortion in these complexes will decrease some of the vibronic interactions. Altogether and without experimental data and/or quantum dynamics simulations for these molecules it is difficult to conclude as to the consequences of the phen substitution on the ultrafast S3 to T1 decay.

From the above considerations we may expect concurrent elementary processes to occur upon irradiation in the MLCT band at about 490 nm. The branching ratio between the different scenario will depend on the experimental conditions and ligand substitutions. We have to distinguish between highly symmetric molecules with small steric constraints (complexes $\mathbf{1}_H$, $\mathbf{1}_{Me}$), for which flattening nearly inhibits luminescence and sterically-demanding molecules as complex $\mathbf{1}_{tBu}$ is characterized by significant quantum yields ($\phi^{em} > 10^{-2}$) and rather long lifetimes (a few hundred of ns), challenging the $[\text{Ru}(\text{bpy})_3]^{2+}$ complex. These case studies, although well documented, are not fully rationalized and fail at explaining the differences in observed quantum yields and lifetimes.

Quantum dynamics simulations are too prohibitive to be performed systematically on the molecules described here, so we scrutinized the cuts of the PES associated with the

seven low-lying active excited states discussed above as a function of the Cu–X distances (C_{2v} symmetry constraint), the X_1 –Cu– X_2 rocking angle (C_s symmetry constraint) and the C_1 – X_1 – X_2 – C_2 dihedral angle (D_2 symmetry constraint) (Scheme 2).

3.2.2. Calculated Potential Energy Curves Associated with the Low-Lying Excited States and Their Spin–Orbit Interactions

A spin-vibronic mechanism is controlled by the distortions at Franck–Condon that induce intrastate coupling leading to a shift of the excited state potentials in position and in energy. This generates critical geometries favorable to efficient non-adiabatic transitions induced by vibronic and SO couplings. Let us examine the case study of complex **1_H** and the cuts of PES depicted in Figure 4 for this D_{2d} molecule. It should be kept in mind that in the D_{2d} structure the HOMO is of e symmetry (doubly degenerate orbital) as well as the LUMO, generating degenerate S1 and T1 states. Upon geometry distortion, the symmetry is reduced and the degeneracy is lifted. This has no effect on the PES curve (Figure 4) but has some influence on the SOC curves (Figure 5). The S1–T1 SOC is nil for the breathing and rocking modes but not for the flattening due to the electronic reorganization in the excited states upon symmetry reduction.

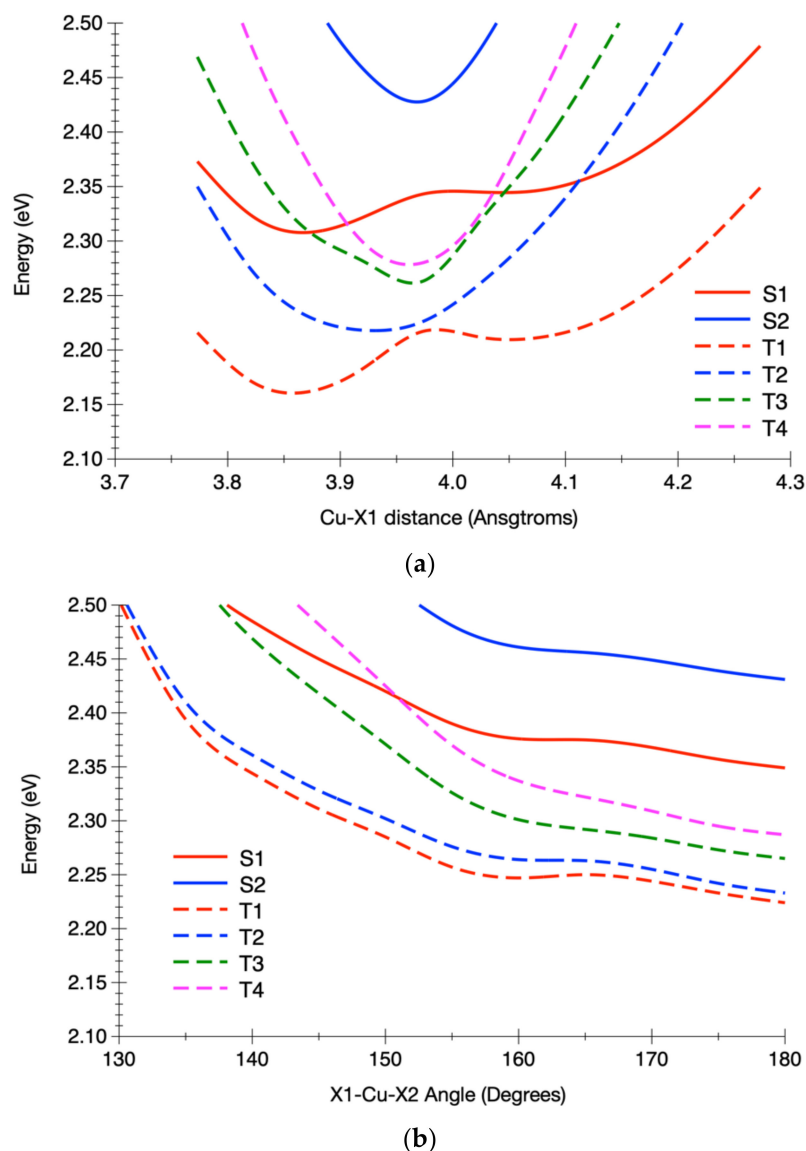


Figure 4. Cont.

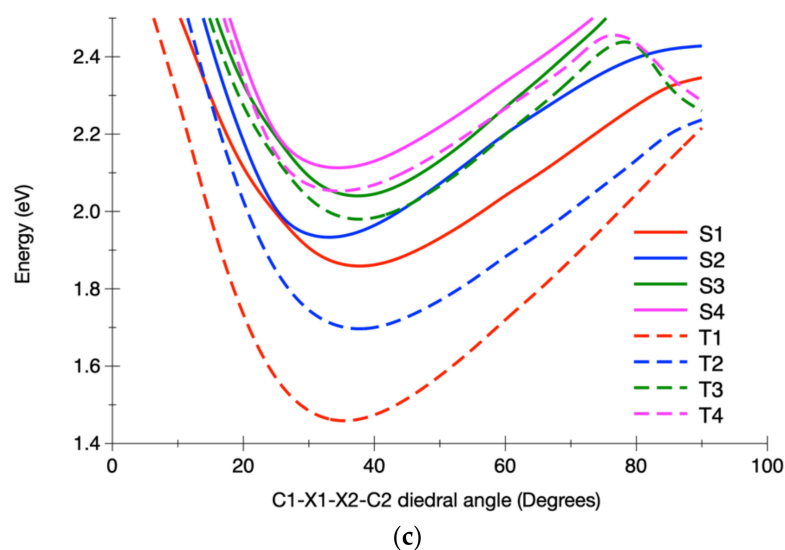


Figure 4. One-dimensional cuts of the PES associated with the low-lying singlet and triplet excited states of 1_H as a function of the breathing mode (Cu–X) (a), the angular distortion (X–Cu–X) (b) and the flattening mode (c), as defined in Scheme 2.

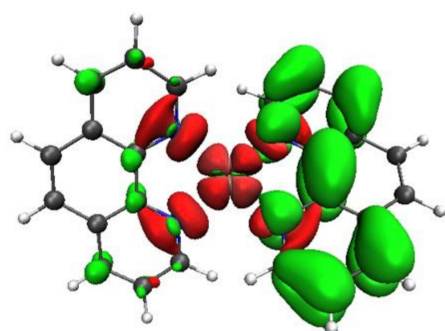


Figure 5. Electron density difference maps for the vertical transition $S_1 \rightarrow S_0$, computed at the S_1 minima for 1_H . Electron density-enriched and -depleted areas are in green and red, respectively.

The breathing of the phen ligands clearly induces the stabilization of S_1 and T_1 with the formation of two minima at Cu–X = 3.87 Å and 4.07 Å, corresponding to the exciton delocalization on one or the other phen (Figures 4a and 5). Several crossings between S_1 and T_4 , T_3 and T_2 will favor an ultrafast population of these triplet states. Moreover, the near-degeneracy between T_2 and T_1 at 3.97 Å is promising for an efficient population of T_1 (Figure 3). The rocking angle X_1 –Cu– X_2 deformation does not modify the ordering of the low-lying excited states and the associated PEC are nearly flat (Figure 4b). More interestingly, the dihedral deformation C_1 – X_1 – X_2 – C_2 associated with the flattening of the molecule drastically destabilizes the T_3 and T_4 excited states and significantly stabilizes the S_1 , T_2 and T_1 states (Figure 4c). The large S_1 – T_2 SOC at Frank–Condon and the increase of T_1 – T_2 SOC as function of Cu–X with two maxima at 3.87 Å and 4.07 Å, combined with small S_1 – T_1 and S_1 – T_2 energy gaps (<0.15 eV) (Figure 6), favor a T_2 / T_1 exchange of population at the early time (<1 ps), as observed experimentally [38]. These ultrafast processes have been rationalized theoretically by means of dynamics simulations [44,50].

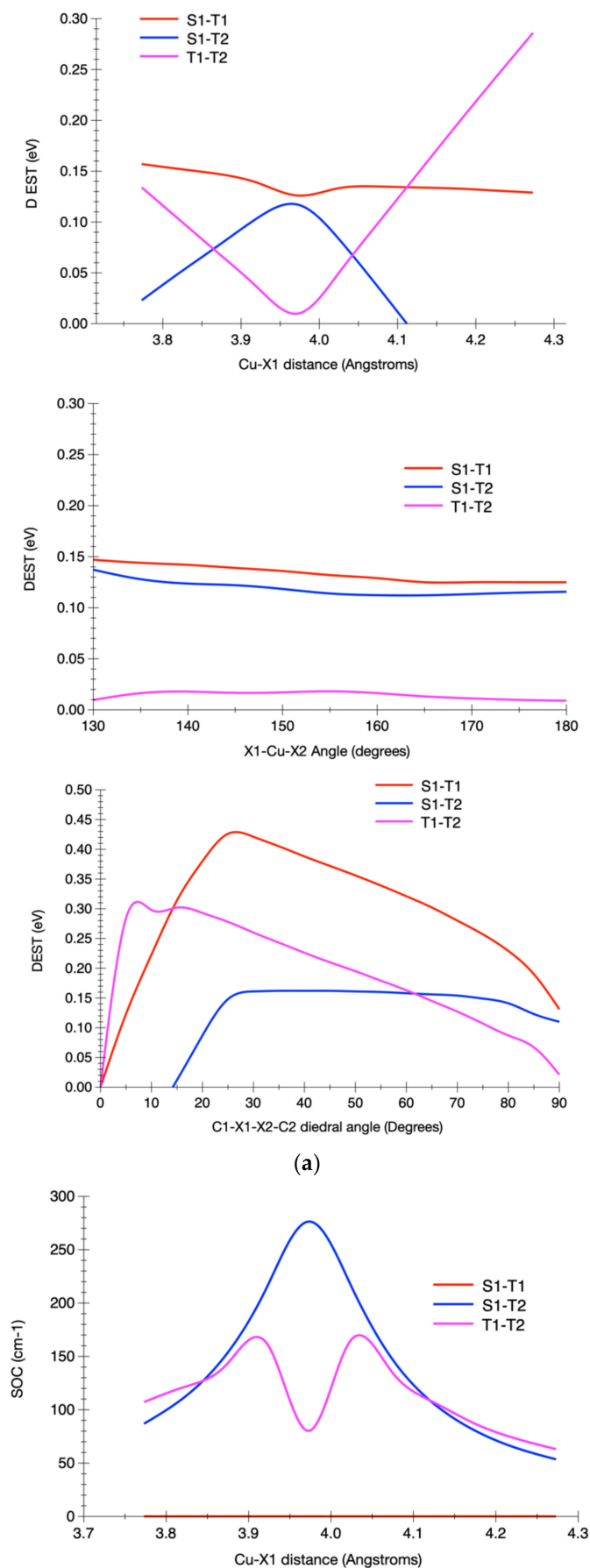


Figure 6. Cont.

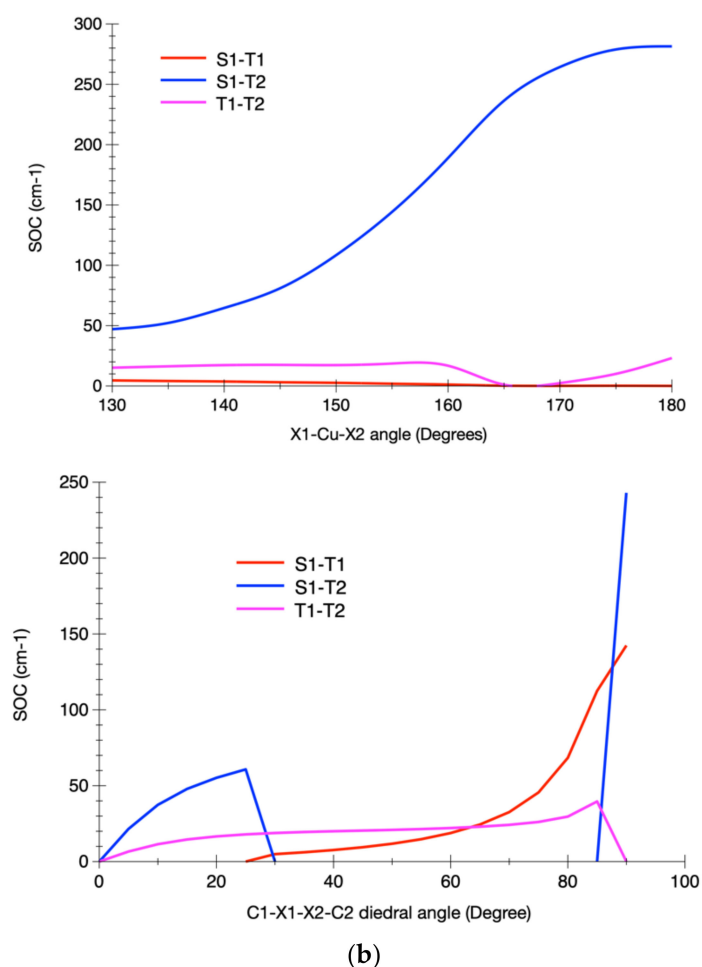


Figure 6. Evolution of the singlet–triplet energy gaps (a) and SOC (b) of $1H$ as a function of the breathing mode (Cu–X), the angular distortion (X–Cu–X) and the flattening mode, as defined in Scheme 2. The discontinuity on the SOC values for the dihedral angles is due to the crossing between S1 and S2 around 25° .

It seems clear that only S1, T2 and T1 will be involved at the longer time-scales ($>$ a few ps) that control the luminescence quantum yields and lifetimes. The parameters which govern the different mechanisms and the branching ratio between them, namely S1–S0 fluorescence, T1–S0 phosphorescence, indirect TADF and non-radiative decay, are the oscillator strengths; the S1/T1, S1/T2 and T1/T2 SOC; the S1–T1, S1–T2 and T1–T2 ΔE energy gaps and their evolution as functions of the structural deformations.

A TADF mechanism is excluded for $1H$ because S1–T1 SOC is null and the flattening induces both a large increase of the S1–T1 energy gap and a significant decrease of the S1–S0 oscillator strength. The only possibility of a back population of S1 would be via the T2 state driven by a small S1–T2 energy gap and a significant S1/T2 SOC at the equilibrium structure. However, the structural deformations, both the distortion and the flattening, do not induce important S1/T1 SOC, reduce S1/T2 SOC and increase the energy gaps (Figure 6).

At the T1 optimized structure, the spin–orbit state E1, E2 and E3 oscillator strengths vary drastically as functions of the key nuclear coordinates (Scheme 2), as illustrated in Figure 7. The flattening (Figure 7c) quenches the phosphorescence. Moreover, according to the data reported in Table 6 for $1H$, the calculated emission wavelengths associated with S1 \rightarrow S0 and T1 \rightarrow S0 are too low to make these transitions radiative.

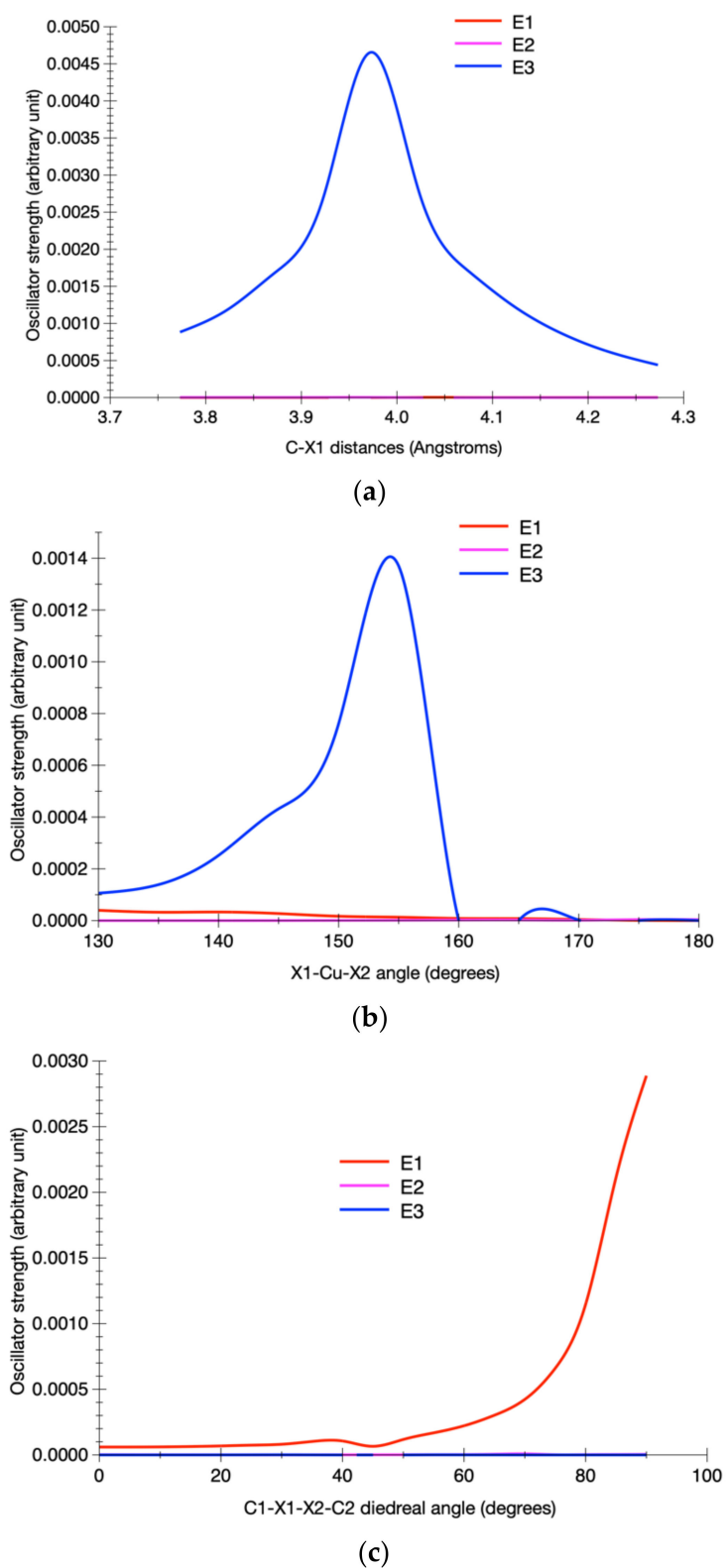


Figure 7. Evolution of the E1, E2 and E3 spin-orbit state oscillator strengths of the three components of the T1 state of $\mathbf{1}_H$ as a function of the breathing mode (a), the angular distortion (b) and the flattening mode (c), as defined in Scheme 2.

Table 6. Deformation, emission and stabilization energies (in eV), emission wavelengths (in nm), singlet–triplet energy gaps (in eV), SOC (in cm^{-1}) and oscillator strengths at the S1 and T1 optimized structures of $\mathbf{1}_H$, $\mathbf{1}_{Me}$ and $\mathbf{1}_{tBu}$ (δ).

State		$\mathbf{1}_H$	$\mathbf{1}_{Me}$	$\mathbf{1}_{tBu}$ (δ)
S1	E_{def}	0.820	0.442	0.253
	E_{em}	0.707	1.569	1.813
	E_{stab}	1.527	2.011	2.066
	λ_{em}	1753	790	684
	f_{osc}	2.25×10^{-5}	1.77×10^{-2}	2.54×10^{-4}
T1	E_{def}	0.610	0.443	0.307
	E_{em}	0.704	1.246	1.656
	E_{stab}	1.314	1.689	1.964
	λ_{em}	1761	995	749
	ΔE_{ST}	0.464	0.411	0.143
	SOC S1–T1	25.5	54.2	20.1
	f_{osc}	2.28×10^{-9}	2.01×10^{-9}	6.85×10^{-6}
	7.01×10^{-9}	5.38×10^{-8}	2.77×10^{-5}	
	2.34×10^{-6}	1.17×10^{-4}	1.77×10^{-4}	

Let us focus now on the $\mathbf{1}_{tBu}$ complex, in which the flattening is nearly inhibited. The only allowed substantial structural deformation is the breathing, which generates S1 and T1 potentials characterized by two minima, in a manner similar to $\mathbf{1}_H$ but totally dissymmetric with one potential well at 3.90 Å, where the system can be trapped either in S1 or in T1 (Figure 8).

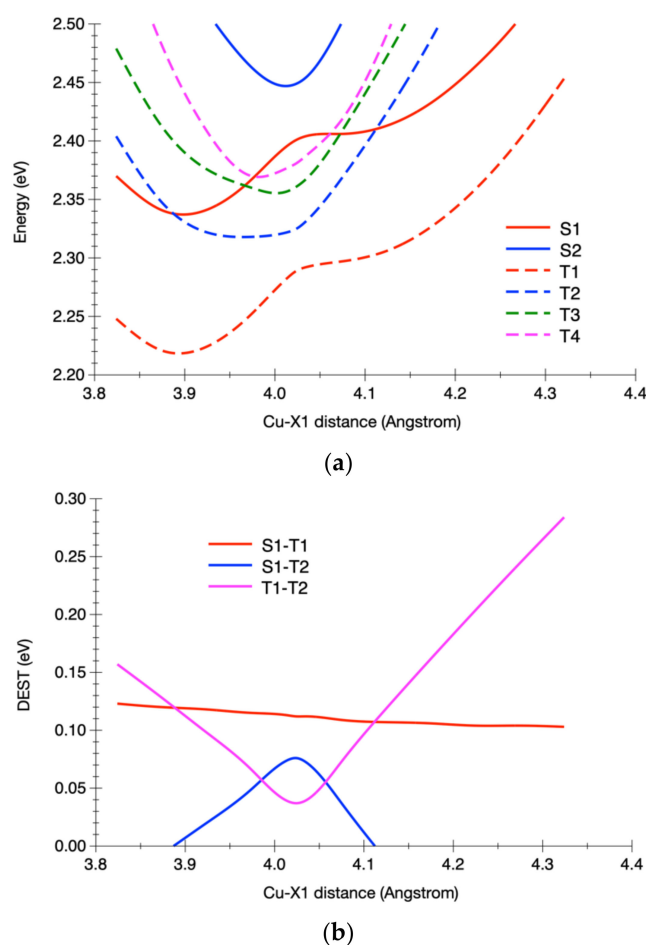


Figure 8. Cont.

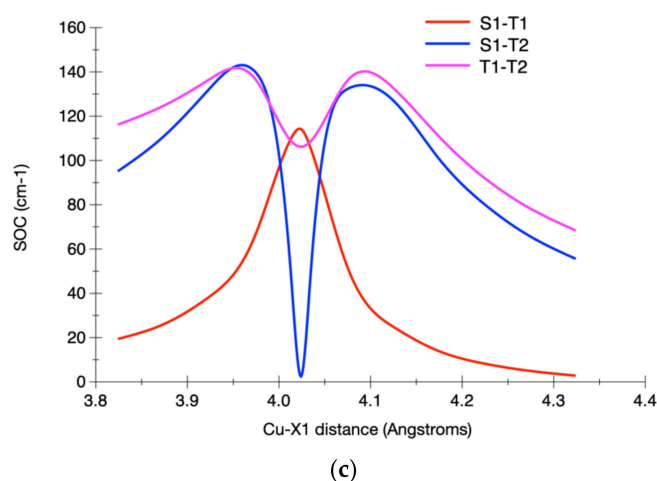


Figure 8. One-dimensional cuts of the PES associated with the low-lying singlet and triplet excited states (a), evolution of the singlet–triplet energy gaps (b) and SOC (c) of $\mathbf{1}_{\text{tBu}}$ as a function of the breathing mode (Cu–X), as defined in Scheme 2.

In $\mathbf{1}_{\text{tBu}}$, $\Delta E_{\text{S1-T1}}$ amounts to 0.12 eV on average with very small variations and the symmetry breaking activates S1/T1 SOC. In addition, the structural deformation generates a S1/S0 oscillator strength of $\sim 10^{-3}$ in $\mathbf{1}_{\text{tBu}}$ as compared to $\sim 10^{-13}$ in $\mathbf{1}_{\text{H}}$. At Franck–Condon, the S1–T1 SOC is large, warranting the efficient population of T1. As soon as T1 is populated the system evolves to the T1 minimum at 3.90 Å, where S1 (Figure 9) can be back populated through S1–T1 SOC, assisted by large T1/T2 and S1/T2 SOC (Figure 8a). Consequently, the system may be the seat of T1 \rightarrow S0 phosphorescence and of both direct (at Franck–Condon) and TADF (at 3.90 Å) S1 \rightarrow S0 fluorescence. The contribution of T2 to the phosphorescence cannot be excluded. This explains the unique photophysical properties of $\mathbf{1}_{\text{tBu}}$ developed after absorption at 425 nm, namely a long-lived MLCT emission (λ_{em} , 599 nm; τ , 3260 ns) and the largest quantum yield (ϕ , 5.6%) of all $[\text{Cu}(\text{R}_2\text{phen})_2]^+$ complexes [53]. This mechanism, corroborated by the data reported in Table 6 for $\mathbf{1}_{\text{tBu}}$, namely the deformation, emission and stabilization energies, emission wavelengths, singlet–triplet energy gaps, SOC and oscillator strengths at the excited state optimized structures, explains the occurrence of a superposition of phosphorescence and TADF contributions in the steady-state emission spectra as discussed experimentally for a number of new sterically-hindered complexes [54,88–90].

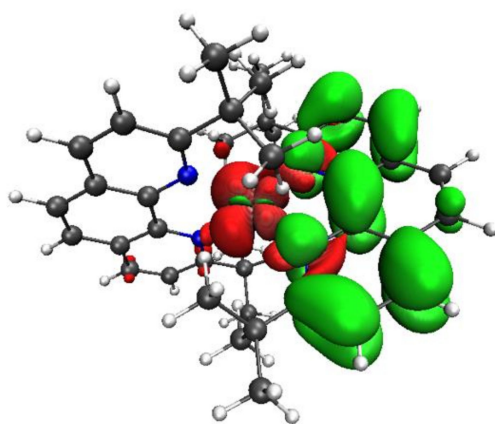


Figure 9. Electron density difference maps for the vertical transition $\text{S}_1 \rightarrow \text{S}_0$, computed at the S_1 minima for $\mathbf{1}_{\text{tBu}}$. Electron density enriched and depleted areas are in green and red, respectively.

The proposed mechanism for the two case studies reported above, namely $\mathbf{1}_{\text{H}}$ and $\mathbf{1}_{\text{tBu}}$, may be drastically modified by the experimental conditions (solvent, temperature, etc.). This points to the weakness of the two-state S1/T1 model based on frontier molecular

orbitals defined for one minimum. The presence of six identified conformers in the ground state PES of **1**_{tBu} (α , β , γ , δ , ϵ and ζ , Scheme 3), multiplied by two in the S1 and T1 excited states (by breathing motion, Table S11) thwarts the above mechanism on a long time-scale. Based on the low calculated energy barriers (<7 kcal mol⁻¹) the free rotation of the tBu groups in solution and the thermal distribution of the different conformers are ensured (Table 7).

Table 7. Symmetry, deformation (E_{def}), emission (E_{em}) and stabilization (E_{stab}) of energies in eV and the relative stability of the different conformers (ΔE in eV), emission wavelength (λ_{em} in nm), S1–T1 splitting (ΔE_{ST} in eV), S1–T1 SOC (in cm⁻¹) and oscillator strength at S1 and T1 optimized geometries for **1**_{tBu}.

State	Conformer	α	β	γ	δ	ϵ	ζ
	GS Symmetry	D _{2d}	D _{2d}	C ₁	C ₂	C ₁	C _{2v}
S1	S1 Symmetry	C ₂	C ₂	C ₁	C ₁	C ₁	C ₂
	E_{def}	0.542	0.497	0.279	0.286	0.376	0.249
	E_{em}	1.944	1.779	1.870	1.813	1.801	1.884
	E_{stab}	2.486	2.275	2.149	2.099	2.177	2.133
	ΔE	0.387	0.176	0.050	0.000	0.078	0.033
	λ_{em}	638	697	663	684	688	658
	f_{osc}	1.06×10^{-5}	1.57×10^{-6}	1.53×10^{-5}	2.54×10^{-4}	2.53×10^{-5}	1.59×10^{-8}
	T1 Symmetry	C ₂	C ₂	C ₁	C ₁	C ₁	C ₂
T1	E_{def}	0.585	0.513	0.295	0.341	0.397	0.270
	E_{em}	1.745	1.633	1.715	1.656	1.648	1.726
	E_{stab}	2.331	2.146	2.011	1.997	2.046	1.997
	ΔE	0.334	0.149	0.014	0.000	0.049	0.000
	λ_{em}	710	759	723	749	752	718
	ΔE_{ST}	0.188	0.133	0.144	0.143	0.138	0.140
	SOC S1–T1	73.0	6.0	3.6	20.1	8.3	0.0
	f_{osc}	3.04×10^{-6}	2.10×10^{-9}	7.05×10^{-7}	6.85×10^{-6}	4.25×10^{-6}	1.09×10^{-13}
		8.97×10^{-6}	6.86×10^{-6}	4.69×10^{-5}	2.77×10^{-5}	1.42×10^{-5}	6.25×10^{-6}
		3.04×10^{-4}	3.01×10^{-4}	2.81×10^{-4}	1.77×10^{-4}	2.46×10^{-4}	2.88×10^{-4}

The emission properties (deformation, emission, stabilization energies, emission wavelengths, oscillator strengths, S1–T1 energy splitting and SOC) computed at S1 and T1 minima are reported in Table S11. The C₁ symmetry of the T1 state originated from the δ conformer warrants a significant S1–T1 SOC (10.1 cm⁻¹) and a small S1–T1 splitting (0.143 eV) favorable to TADF associated with a highly emissive S1 state ($f > 10^{-4}$). In contrast the T1 and S1 states generated by the conformer ζ are of C₂ symmetry, resulting in the C_{2v} symmetry reduction in the ground state structure. If the S1–T1 splitting (0.140 eV) is unaffected in the ζ conformer, the S1–T1 SOC is inhibited despite this small symmetry breaking (Table S11), which deactivates the TADF mechanism. Moreover, the low oscillator strength of S1 ($f < 10^{-7}$) does not support fluorescence. Due to its stability, the ζ conformer is undoubtedly present in the solution and contributes to the emission properties either by phosphorescence or by non-radiative decay. Another possibility is that ζ plays the role of a reservoir: by tBu rotation it may evolve to the γ , δ and ϵ conformers reactivating the SOC and, thus, the TADF mechanism.

The co-existence of several conformers in the solution drastically complicates the mechanism due to the presence of shallow minima in the PES associated with S1, T1 and S0 accessible on a longer time-scale. Moreover, we may expect conformer specific ultrafast decay channels, as observed in some organic chromophores [91].

Whereas the ultrafast population of the low-lying S1, T2 and T1 excited states is well documented, both theoretically and experimentally for **1**_H, the longer time-scale non-adiabatic dynamics, including spin-vibronic effects and involving these three key states,

has to be discovered. The present study paves the way to more sophisticated dynamical simulations in the ns time-scale.

3.3. Towards Supramolecular Design

Despite its remarkable photophysical properties, the *tertio*-butyl-substituted complex **1_{tBu}** suffers from serious drawbacks, namely instability in various solvents [53]. The steric congestion due to the *tertio*-butyl groups favors the decoordination of one of the substituted phen by a solvent molecule (as CH₃CN). This can be illustrated by the calculated complexation energies of the second phen onto the [Cu(phen)]⁺ complex to give [Cu(phen)₂]⁺. The ΔG of complexation amounts to -31.6 kcal mol⁻¹ for **1_H** and -38.5 kcal mol⁻¹ for **1_{Me}** but decreases to -19.8 kcal mol⁻¹ for **1_{tBu}** (computed with GAUSSIAN, in CH₃CN). In light of the performance of **1_{tBu}**, other functionalizations of the phen have been explored in position 2 and 9 of the phen to prevent flattening by steric congestion. However, none of the tested complexes exhibit performances similar to **1_{tBu}**. For instance, inter-ligand interactions may cause flattening even in the singlet ground state, as with 2,9-diphenylphenantroline [92,93]. To the best of our knowledge, no example of flattening blocked due to the linkage of the two ligands exists, while partial linkage has been explored [56,94,95]. We present here two promising structures illustrating this possibility. They derive from the structure ζ of **1_{tBu}**, a link being created between the alkyl groups of position 2 of the two phens. The same link is created with the groups in position 9 (Scheme 1). We propose complex **2** (Scheme 1), in which a C_{2v} symmetry is retained, and complex **3**, which is asymmetric due to the presence of an isopropyl group.

3.3.1. Complex 2

The linkage constrains the geometry and make the two phen core inequivalent, due to the different orientations of the methyl groups in the linker. Two methyl point towards the copper center and two methyl point outside the complex (Figure 10). The Cu–N distances are significantly larger than in **1_H** and **1_{Me}**, being close to those in **1_{tBu}** (Table S11). The X₁–Cu–X₂ and C₁–X₁–X₂–C₂ angles fit the ideal values, namely 180° and 90°, respectively. The absorption spectrum of **2** is very close to that of **1_{tBu}** (Figure 1) with similar transitions (Figures 2 and 3).

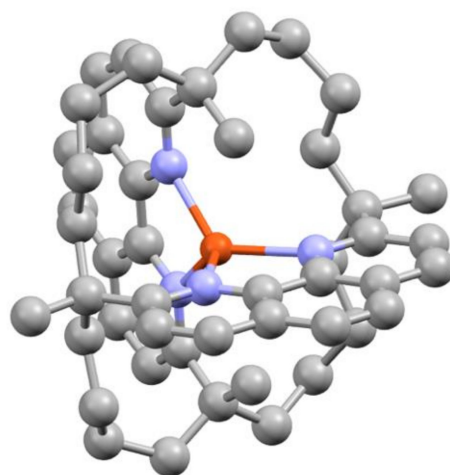


Figure 10. Optimized structure of **2**, hydrogen atoms are omitted for clarity.

Upon excitation, the structural rigidity imposed by the linker leads to the retention of the C_{2v} symmetry. As for the previous complexes, the lowest excited states are mainly MLCT, and the electron transferred to the ligand is localized on one of the phen and generates two almost degenerate minima on the lowest S₁ and T₁ PESs (Table S13). All the structures belong to the A₂ symmetry point group and their photophysical characteristics are presented in Table 8. They are very close to those of the ζ form of **1_{tBu}** with a small

singlet–triplet gap ($\Delta E_{ST} = 0.135$ eV) at T1 geometry. However, due to the A2 symmetry of T1 and S1, the SOC S1–T1 is strictly zero, deactivating the TADF mechanism. Furthermore, the oscillator strength associated with S1 is also zero. This first structure proves that the introduction of linkers between the two phen ligands induce structural rigidity preventing any flattening. This results in a small ΔE_{ST} similar to those computed with $\mathbf{1}_{tBu}$. However, the C_{2v} symmetry of the excited singlet and triplet state disfavors the TADF mechanism by cancelling the SOC between S1 and T1 and the oscillator strength of S1.

Table 8. Deformation, emission and stabilization energies (in eV), emission wavelengths (in nm), singlet–triplet energy gaps (in eV), SOC (in cm^{-1}) and oscillator strengths at the S1- and T1-optimized structures of **2** and **3**.

State		2	2	3	3
S1	E_{def}	0.227	0.241	0.257	0.343
	E_{em}	1.783	1.797	1.881	1.893
	E_{stab}	2.009	2.037	2.137	2.235
	λ_{em}	695	690	659	655
	f_{osc}	0.00	0.00	5.43×10^{-5}	5.73×10^{-6}
T1	E_{def}	0.243	0.26	0.277	0.365
	E_{em}	1.634	1.643	1.717	1.733
	E_{stab}	1.877	1.903	1.995	2.098
	λ_{em}	759	754	722	715
	ΔE_{ST}	0.135	0.138	0.146	0.143
	SOC S1–T1	0.0	0.0	7.7	2.9
	f_{osc}	9.96×10^{-8}	1.04×10^{-7}	2.37×10^{-7}	1.28×10^{-8}
	4.81×10^{-6}	1.07×10^{-5}	5.68×10^{-6}	3.87×10^{-6}	
	3.03×10^{-4}	1.39×10^{-4}	3.10×10^{-4}	1.51×10^{-4}	

3.3.2. Complex 3

The structure of cage **2** is of C_{2v} symmetry, and similarly to the ζ conformer of $\mathbf{1}_{tBu}$, this disfavors emission. The emission properties of $\mathbf{1}_{tBu}$ are due to its asymmetric conformers. We modified the structure of **2** by deleting three of the methyl groups of the linker and replacing the fourth one with an isopropyl (Scheme 1) to introduce an asymmetry in complex **3**. The two phen ligands are no longer equivalents (Table S9) and the Cu–N bonds especially are significantly different (2.020 to 2.299 Å) in **3** as compared to **2** (2.140 to 2.156 Å). Furthermore, the phen ligand facing the isopropyl moiety is no longer planar. The absorption spectrum of **3** (Figure 1) is similar in shape to that of **2** but blue-shifted by roughly 50 nm. The nature of the singlet transitions (Figure 2) is the same as in the other complexes, being almost exclusively dominated by MLCTs.

We optimized the lowest excited singlet and triplet states of **3** (Tables 8 and S13, Figure 11). We retrieved the two minima on the S1 and T1 PES, due to the localization of the exciton on each of the phen. The presence of the isopropyl group breaks the symmetry, and the two minima are no longer degenerate. Furthermore, both S1 and T1 minima do not have any symmetry. The consequence is an activation of the SOC between S1–T1 (7.7 cm^{-1}). The linkers, by preventing any flattening of T1 structure (Table S12), retain a small ΔE_{ST} (0.146 eV, Table 8). These values are comparable to that of $\mathbf{1}_{tBu}$ for forms γ , δ or ε (Table S9), which are those contributing to the emission properties of $\mathbf{1}_{tBu}$.

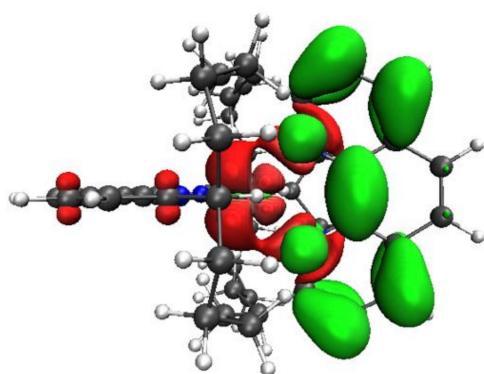


Figure 11. Electron density difference maps for the vertical transition $S_1 \rightarrow S_0$, computed at the S_1 minima for complex 3. Electron density enriched and depleted areas are in green and red, respectively.

4. Discussion

The emission properties of the $[\text{Cu}(\text{phen})_2]^+$ class of complexes is governed by the TADF mechanism, namely a back-population of S_1 from T_1 . This process depends on two critical parameters, the spin–orbit coupling and the energy splitting between S_1 and T_1 in the simplest case. Upon excitation, the lowest excited state of these complexes is a MLCT from the copper cation towards the ligand, which induces nuclear relaxation. Two main motions (Scheme S1) are involved. First, the formal electronic state of the copper is Cu^{2+} , with only nine electrons in the 3d shell, this leads to the rotation of the phen ligand to form a planar complex, with a half-filled $3d_{x^2-y^2}$ orbital (the “flattening”). This is the first motion. The second one is due to the localization of the excited electron on the ligand. In the Franck–Condon geometry, the electron is generally delocalized on the two phen. However, upon relaxation, there is a breathing of the Cu–N bonds due to the change of Cu formal oxidation state associated with the localization of the excited electron on only one of the phen (“the breathing”). This potentially generates two minima, as the excited electron could be on one or the other phen. The minima are degenerate if the two phen are identical, and if they are asymmetric, degeneracy is lifted. In addition to these two motions, a last point has to be considered. Indeed, with complex ligands, the conformational flexibility has to be taken into account. $\mathbf{1}_{\text{tBu}}$ is a good example with several conformers generated by the relative orientation of the tertio-buthyl groups, each conformer exhibiting its own emission properties. The experimental values are the results of the contribution of the conformers thermal distribution.

The flattening is associated with an increase in the ΔE_{ST} , which disfavors TADF and paves the way to phosphorescence or non-radiative decay. We also observe a decrease in the S_1 – T_1 SOC. The changes associated with the breathing are less important, the variations of the ΔE_{ST} are negligible but the SOC decreases with the distortion of the structure. The prevention of the flattening and limitation of the breathing are mandatory to retain good emission properties. This is achieved with $\mathbf{1}_{\text{tBu}}$, which bulky tertio-butyl groups makes flattening impossible and is associated with the best emission performances. Less bulky CH_3 groups in $\mathbf{1}_{\text{Me}}$ lead to significant flattening with poor emission and $\mathbf{1}_{\text{H}}$ is not emissive. However, the bulkiness of the tertio-butyl groups is the source of inter-ligand repulsion, destabilizing the complex. In a coordinative solvent, such as CH_3CN , one of the ligands may be substituted by solvent molecule. To overcome this problem, many complexes have been synthesized with less bulky substituents. However, if the complex stability increases, the less sterically hindered complex leads to significant flattening, weakening the emission performance. The reason for this flattening is that the substituent can adapt its position, as observed with isopropyl [96]. For the latter, the isopropyl rotate and allows a significant flattening. An extreme case can be seen in phenyl rings instead of tertio-butyl, in this complex the structure is flattened even in the ground state [92,93]. All the proposed structural modifications rely on the geometry constraints due to substituent repulsion to maintain a geometry close to Franck–Condon geometry in the excited state.

An alternative path is possible by linking the phen ligand together. Some structures have been synthesized but not with linkers between the phens on the same complex. Our detailed theoretical study led to promising molecules with emission characteristics tailored by symmetry breaking and spin-orbit coupling. Due to the structural rigidity, the complex should be stable in a standard solvent, with the departure of one of the phen requiring the departure of both of them. The flattening in excited states is prevented here by linkers instead of steric repulsion. Consequently, the S1–T1 energy gap remains small in complexes **2** and **3** and compares to the calculated value in **1_{tBu}**. However, as shown in **1_{tBu}**, structures that are too symmetric and close to C_{2V} , are not in favor of efficient emission, as illustrated by complex **2** or by some conformers of **1_{tBu}**. Complex **3**, with its asymmetric linkers, exhibits the most promising emission characteristics.

5. Conclusions

We report here a complete computational study of the structural, optical and photophysical properties of copper(I) phenanthroline-functionalized complexes, including solvent and spin-orbit coupling effects. The study focusses on the parameters which govern the different decay mechanisms and the branching ratio between them, namely S1–S0 fluorescence, T1–S0 phosphorescence, indirect TADF and non-radiative process. For this purpose, the oscillator strengths, the S1/T1, S1/T2 and T1/T2 spin-orbit interactions as well the S1–T1, S1–T2 and T1–T2 energy gaps are calculated as a function of the structural deformations of the complexes. More specifically, three modes are important: the Cu–X breathing, the X–Cu–X angular distortion (X being the center of the functionalized phen ligands) and the flattening mode. A TADF mechanism is excluded for $[Cu(I)(phen-R_2)_2]^+$ (R=H, methyl) because of a null S1–T1 SOC, a large S1–T1 energy gap and a significant decrease in S1–S0 oscillator strength induced by flattening. Radiative processes are hindered as well. The inhibition of the flattening in $[Cu(I)(phen-R_2)_2]^+$ (R = *tertio*-butyl) and the identification of six conformers in its electronic ground state, generating twelve local minima in the S1 and T1 potential energy surfaces along the breathing mode lead to a complex mechanism. At the early time, a large S1–T1 SOC activated by symmetry breaking, a small S1–T1 energy gap and a large S1/S0 oscillator strength spawned by structural deformation are in favor of both direct fluorescence (at Franck–Condon) and TADF. An efficient phosphorescence is expected from T1 with a potential contribution of T2. At longer time-scales the co-existence of several conformers in solution drastically complicates the mechanism. These features explain the unique photophysical properties of *tertio*-butyl complex as well as the occurrence of the superposition of phosphorescence and TADF contributions in newly synthesized sterically hindered complexes.

In order to overcome the drawback of instability in solution, the consequence of the decoordination of one phen by a solvent molecule, two complexes with promising photophysical properties are proposed. The new structures are derived from the C_{2V} conformer ζ of the *tertio*-butyl substituted Cu(I) complex by linking the two phen in positions 2 and 9 (complex **2**). The introduction of asymmetry (complex **3**) by appropriate linkers leads to the most interesting molecular cage in terms of photophysical characteristics paving the way for a new supramolecular design.

Supplementary Materials: The following supporting information can be downloaded at: <https://www.mdpi.com/article/10.3390/ma15155222/s1>, Figure S1: In (left) and out (right) orientations of a tBu group on a simplified complex holding only one tBu; Figure S2: ADF computed Absorption spectra for the different conformers of **1_{tBu}**; Figure S3: Frontier orbitals of **1_H** and energies in eV; Figure S4: Frontier orbitals of **3** and energies in eV; Scheme S1: Representation of the four possible Triplet minima after irradiation of **1_{Me}** complex. In bold blue are the long Cu–N distance, in bold red the short Cu–N distance and in purple the indication of how the phen ligands is out of plane.; Table S1: Experimental (from CSD reference) and computed (GAUSSIAN) geometrical parameters for complex **1_H**. Distances are in Angstroms, angles and dihedral angles in degrees; Table S2: Experimental (from CSD reference) and computed (GAUSSIAN) geometrical parameters for complex **1_{Me}**. Distances are in Angstroms, angles and dihedral angles in degrees; Table S3: Computed (GAUSSIAN) geometrical

parameters for complexes **1_{tBu}**, **2** and **3** in the ground state. Distances are in Angstroms, angles and dihedral angles in degrees; Table S4: Experimental geometrical parameters for complex **1_{tBu}**. Distances are in Angstroms, angles and dihedral angles in degrees; Table S5: Computed (GAUSSIAN) geometrical parameters for complexes in the triplet state. The values are given for conformer δ for **1_{tBu}**. Distances are in Angstroms, angles and dihedral angles in degrees and energies in kcal mol⁻¹; Table S6: Selected nuclear coordinates at the optimized ground state and low-lying excited states for **1H** computed with ADF. Distances are in Angstroms, angles and dihedral angles in degrees; Table S7: Selected nuclear coordinates at the optimized ground state and low-lying excited states for **1_{Me}** computed with ADF. Distances are in Angstroms, angles and dihedral angles in degrees; Table S8: Selected nuclear coordinates at the optimized ground state and low-lying excited states for **1_{tBu}** for experimental δ structure computed with ADF. Distances are in Angstroms, angles and dihedral angles in degrees; Table S9: Computed ground state (ADF) geometrical parameters. Distances are in Angstroms, angles and dihedral angles in degrees; Table S10: Selected nuclear coordinates at the low-lying excited states for **1_{tBu}** computed with ADF. Distances are in Angstroms, and angles in degrees; Table S11: Emission data computed with ADF for S1 and T1 states of **1_{tBu}**. E_{def} , E_{em} , E_{stab} , ΔE and ΔE_{ST} are in eV, λ_{em} is in nm, SOC is in cm⁻¹. 1) Values for the 2nd minima due to oscillation of the exciton for γ , ϵ and ζ . Data are not given for α , β and δ because the second minima is strictly identical to the first one due to symmetry; Table S12: Spin-orbit coupling (in cm⁻¹) between the low-lying excited states in **1_{Me}** computed with ADF; Table S13: Computed S1 and T1 (ADF) geometrical parameters. Distances are in Angstroms, angles and dihedral angles in degrees. References [73–87] are cited in the Supplementary Materials.

Author Contributions: Writing—original draft, C.G. and C.D. All authors have read and agreed to the published version of the manuscript.

Funding: This research received no external funding.

Institutional Review Board Statement: Not applicable.

Informed Consent Statement: Not applicable.

Acknowledgments: The calculations were carried at the Strasbourg computing center (HPC).

Conflicts of Interest: The authors declare no conflict of interest.

References

1. Buckner, M.T.; McMillin, D.R. Photoluminescence from copper(I) complexes with low-lying metal-to-ligand charge transfer excited states. *J. Chem. Soc. Chem. Commun.* **1978**, 759–761. [[CrossRef](#)]
2. Blaskie, M.W.; McMillin, D.R. Photostudies of copper(I) systems. 6. Room-temperature emission and quenching studies of bis(2,9-dimethyl-1,10-phenanthroline)copper(I). *Inorg. Chem.* **1980**, *19*, 3519–3522. [[CrossRef](#)]
3. Rader, R.A.; McMillin, D.R.; Buckner, M.T.; Matthews, T.G.; Casadonte, D.J.; Lengel, R.K.; Whittaker, S.B.; Darmon, L.M.; Lytle, F.E. Photostudies of [Cu(bpy)(PPh₃)₂]⁺, [Cu(phen)(PPh₃)₂]⁺, and [Cu(dmp)(PPh₃)₂]⁺ in Solution and in Rigid, Low-Temperature Glasses. Simultaneous Multiple Emissions from Intraligand and Charge-Transfer States. *J. Am. Chem. Soc.* **1981**, *103*, 5906–5912. [[CrossRef](#)]
4. Kirchoff, J.R.; Gamache, R.E., Jr.; Blaskie, M.W.; Del Paggio, A.A.; Lengel, R.K.; McMillin, D.R. Temperature dependence of luminescence from Cu(NN)²⁺ systems in fluid solution. Evidence for the participation of two excited states. *Inorg. Chem.* **1983**, *22*, 2380–2384. [[CrossRef](#)]
5. Kutal, C. Spectroscopic and photochemical properties of *d*¹⁰ metal complexes. *Coord. Chem. Rev.* **1990**, *99*, 213–252. [[CrossRef](#)]
6. Sabin, F.; Ryu, C.K.; Ford, P.C.; Vogler, A. Photophysical properties of hexanuclear copper(I) and silver(I) clusters. *Inorg. Chem.* **1992**, *31*, 1941–1945. [[CrossRef](#)]
7. Li, D.; Che, C.-M.; Wong, W.T.; Shieh, S.J.; Peng, S.M. Luminescent three-co-ordinated dinuclear copper(I) complexes of bis(diphenylphosphino)methane: Photophysical properties and crystal structure. *J. Chem. Soc. Dalton Trans.* **1993**, 653–654. [[CrossRef](#)]
8. Yam, V.W.-W.; Fung, W.K.-M.; Cheung, K.-K. Synthesis, Structure, Photophysics, and Excited-State Redox Properties of the Novel Luminescent Tetranuclear Acetylidocopper(I) Complex [Cu₄(μ-dppm)₄(μ₄-η¹,η²-C{C-})(BF₄)₂]. *Angew. Chem. Int. Ed.* **1996**, *35*, 1100–1102. [[CrossRef](#)]
9. Yam, V.W.-W.; Lo, K.K.-W.; Fung, W.K.-M.; Wang, C.R. Design of luminescent polynuclear copper(I) and silver(I) complexes with chalcogenides and acetylides as the bridging ligands. *Coord. Chem. Rev.* **1998**, *171*, 17–41. [[CrossRef](#)]
10. Miller, M.T.; Karpishin, T.B. Phenylethynyl substituent effects on the photophysics and electrochemistry of [Cu(dpp₂)²⁺ (dpp = 2,9-Diphenyl-1,10-phenanthroline)]. *Inorg. Chem.* **1999**, *38*, 5246–5249. [[CrossRef](#)]

11. Miller, M.T.; Gantzel, P.K.; Karpishin, T.B. A highly emissive heteroleptic copper(I) bis(phenanthroline) complex: $[\text{Cu}(\text{dbp})(\text{dmp})]^+$ (dbp = 2, 9-Di-*tert*-butyl-1,10-phenanthroline; dmp = 2, 9-Dimethyl-1,10-phenanthroline). *J. Am. Chem. Soc.* **1999**, *121*, 4292–4293. [[CrossRef](#)]
12. Yam, V.W.-K.; Lo, K.K.-W. Luminescent polynuclear d^{10} metal complexes. *Chem. Soc. Rev.* **1999**, *28*, 323–334. [[CrossRef](#)]
13. Ford, P.C.; Cariati, E.; Bourassa, J. Photoluminescence properties of multinuclear copper(I) compounds. *Chem. Rev.* **1999**, *99*, 3625–3647. [[CrossRef](#)] [[PubMed](#)]
14. Scaltrito, D.V.; Thompson, D.W.; O'Calaghan, J.A.; Meyer, G.J. MLCT excited states of cuprous bis-phenanthroline coordination compounds. *Coord. Chem. Rev.* **2000**, *208*, 243–266. [[CrossRef](#)]
15. Che, C.M.; Mao, Z.; Miskowski, V.M.; Tse, M.C.; Chan, C.K.; Cheung, K.K.; Phillips, D.L.; Leung, K.H. Cuprophilicity: Spectroscopic and Structural Evidence for Cu–Cu Bonding Interactions in Luminescent Dinuclear Copper(I) Complexes with Bridging Diphosphane Ligands. *Angew. Chem. Int. Ed.* **2000**, *112*, 4250–4254. [[CrossRef](#)]
16. Mao, Z.; Chao, H.Y.; Hui, Z.; Che, C.-M.; Fu, W.-F.; Cheung, K.-K.; Zhu, N. Excited States of Binuclear Copper(I) Phosphine Complexes: Effect of Copper–Ligand and Copper–Copper Interactions on Excited State Properties and Photocatalytic Reductions of the 4,4'-Dimethyl-2,2'-bipyridinium Ion in Alcohols. *Chem. Eur. J.* **2003**, *9*, 2885–2894. [[CrossRef](#)]
17. Pawlowski, V.; Knoer, G.; Lennartz, C.; Vogler, A. Luminescence and Theoretical Studies of $\text{Cu}(\text{tripod})\text{X}$ [tripod = 1,1,1-Tris(diphenylphosphanyl)methyl)ethane; X^- = Halide, Thiophenolate, Phenylacetylde]. *Eur. J. Inorg. Chem.* **2005**, *15*, 3167–3171. [[CrossRef](#)]
18. Peng, R.; Li, D.; Wu, T.; Zhou, X.-P.; Ng, S.W. Increasing Structure Dimensionality of Copper(I) Complexes by Varying the Flexible Thioether Ligand Geometry and Counteranions. *Inorg. Chem.* **2006**, *45*, 4035–4046. [[CrossRef](#)]
19. Armaroli, N.; Accorsi, G.; Cardinali, F.; Listorti, A. Photochemistry and Photophysics of Coordination Compounds: Copper. *Top. Curr. Chem.* **2007**, *280*, 69–115.
20. Barbieri, A.; Accorsi, G.; Armaroli, N. Luminescent complexes beyond the platinum group: The d^{10} avenue. *Chem. Commun.* **2008**, 2185–2193. [[CrossRef](#)]
21. Tsubomura, T.; Tsukuda, T.; Matsumoto, K. Luminescent d^{10} transition metal complexes. *Bull. Jpn. Soc. Coord. Chem.* **2008**, *52*, 29–42. [[CrossRef](#)]
22. Lavie-Combout, A.; Cantuel, M.; Leydet, Y.; Jonusauskas, G.; Bassani, D.M.; McClenaghan, N.D. Improving the photophysical properties of copper(I) bis(phenanthroline) complexes. *Coord. Chem. Rev.* **2008**, *252*, 2572–2584. [[CrossRef](#)]
23. Tsuge, K. Luminescent Complexes Containing Halogeno-bridged Dicopper(I) Unit $\{\text{Cu}_2(\mu\text{-X})_2\}$ ($\text{X} = \text{Cl}, \text{Br}, \text{and I}$). *Chem. Lett.* **2013**, *42*, 204–208.
24. Tsubomura, T.; Kimura, K.; Nishikawa, M.; Tsukuda, T. Structures and photophysical properties of copper(I) complexes bearing diphenylphenanthroline and bis(diphenylphosphino)alkane: The effect of phenyl groups on the phenanthroline ligand. *Dalton Trans.* **2015**, *44*, 7554–7562. [[CrossRef](#)] [[PubMed](#)]
25. Kakizoe, D.; Nishikawa, N.; Fuji, Y.; Tsubomura, T. Photophysical properties of three coordinated copper(I) complexes bearing 1,10-phenanthroline and a monodentate phosphine ligand. *Dalton Trans.* **2017**, *46*, 14804–14811. [[CrossRef](#)] [[PubMed](#)]
26. Wallesch, M.; Volz, D.; Zink, D.M.; Schepers, U.; Nieger, M.; Baumann, T.; Braese, S. Bright Opportunities: Multinuclear Cu^{I} Complexes with N–P Ligands and Their Applications. *Chem. Eur. J.* **2014**, *20*, 6578–6590. [[CrossRef](#)]
27. Giereth, R.; Mengele, A.K.; Frey, W.; Kloss, M.; Stufen, A.; Karnahl, M.; Tschierlei, S. Copper(I) phosphinooxalazine complexes: Impact of the ligand substitution and steric demand on the electrochemical and photophysical properties. *Chem. Eur. J.* **2020**, *26*, 2675–2684. [[CrossRef](#)]
28. Gunaratne, T.; Rodgers, M.A.J.; Felder, D.; Nierengarten, J.-F.; Accorsi, G.; Armaroli, N. Ultrafast dynamics of $\text{Cu}(\text{I})$ -phenanthrolines in dichloromethane. *Chem. Commun.* **2003**, 3010–3011. [[CrossRef](#)]
29. Samia, A.C.S.; Cody, J.; Fahrni, C.J.; Burda, C. The effects of ligand constraints on the metal-to-ligand charge transfer relaxation dynamics in copper (I)-phenanthroline complexes: A comparative study by femtosecond time-resolved spectroscopy. *J. Phys. Chem. B* **2000**, *108*, 563–569. [[CrossRef](#)]
30. Cody, J.; Dennisson, J.; Gilmore, J.; VanDerveer, D.G.; Henary, M.M.; Gabrielli, A.; Sherrill, C.D.; Zhang, Y.; Pan, C.-P.; Burda, C.; et al. X-ray structures, photophysical characterization, and computational analysis of geometrically constrained copper(I)-phenanthroline complexes. *Inorg. Chem.* **2003**, *42*, 4918–4929. [[CrossRef](#)]
31. Kohler, L.; Hayes, D.; Hong, J.Y.; Carter, T.J.; Shelby, M.L.; Fransted, K.A.; Chen, L.X.; Mulfort, K.L. Synthesis, structure, ultrafast kinetics, and light-induced dynamics of CuHETPHEN chromophores. *Dalton Trans.* **2016**, *45*, 9871–9883. [[CrossRef](#)]
32. Kelley, M.S.; Shelby, M.L.; Mara, M.W.; Haldrup, K.; Hayes, D.; Hadt, R.G.; Zhang, X.; Stickrath, A.B.; Ruppert, R.; Sauvage, J.-P.; et al. Ultrafast dynamics of two copper bisphenanthroline complexes measured by X-ray transient absorption spectroscopy. *J. Phys. B-Atom. Mol. Opt. Phys.* **2017**, *50*, 154006. [[CrossRef](#)]
33. Iwamura, M.; Takeuchi, S.; Tahara, T. Substituent effect on the photoinduced structural change of $\text{Cu}(\text{I})$ complexes observed by femtosecond emission spectroscopy. *Phys. Chem. Chem. Phys.* **2014**, *16*, 4143–4154. [[CrossRef](#)]
34. Fransted, K.A.; Jackson, N.E.; Zong, R.; Mara, M.W.; Huang, J.; Harpham, M.R.; Shelby, M.L.; Thunemel, R.P.; Chen, L.X. Ultrafast Structural Dynamics of $\text{Cu}(\text{I})$ -Bicinchoninic Acid and Their Implications for Solar Energy Applications. *J. Physical Chem. A* **2014**, *118*, 10497–10506. [[CrossRef](#)]
35. Shaw, G.B.; Grant, C.D.; Shirota, H.; Castner, E.W.; Meyer, G.J.; Chen, L.X. Ultrafast structural rearrangements in the MLCT excited state for copper(I) bis-phenanthrolines in solution. *J. Am. Chem. Soc.* **2007**, *129*, 2147–2160. [[CrossRef](#)]

36. Iwamura, M.; Takeuchi, S.; Tahara, T. Real-time observation of the photoinduced structural change of bis(2,9-dimethyl-1,10-phenanthroline)copper(I) by femtosecond fluorescence spectroscopy: A realistic potential curve of the Jahn-Teller distortion. *J. Am. Chem. Soc.* **2007**, *129*, 5248–5256. [[CrossRef](#)] [[PubMed](#)]
37. Lockard, J.V.; Kabehie, S.; Zink, J.I.; Smolentsev, G.; Soldatov, A.; Chen, L.X. Influence of Ligand Substitution on Excited State Structural Dynamics in Cu(I) Bisphenanthroline Complexes. *J. Phys. Chem. B* **2010**, *114*, 14521–14527. [[CrossRef](#)] [[PubMed](#)]
38. Iwamura, M.; Takeuchi, S.; Tahara, T. Ultrafast Excited-State Dynamics of Copper(I) Complexes. *Acc. Chem. Res.* **2015**, *48*, 782–791. [[CrossRef](#)]
39. Hua, L.; Iwamura, M.; Takeuchi, S.; Tahara, T. The substituent effect on the MLCT excited state dynamics of Cu(I) complexes studied by femtosecond time-resolved absorption and observation of coherent nuclear wavepacket motion. *Phys. Chem. Chem. Phys.* **2015**, *17*, 2067–2077. [[CrossRef](#)]
40. Gothard, N.A.; Mara, M.W.; Huang, J.; Szarko, J.M.; Rolczynski, B.; Lockard, J.V.; Chen, L.X. Strong Steric Hindrance Effect on Excited State Structural Dynamics of Cu(I) Diimine Complexes. *J. Phys. Chem. A* **2012**, *116*, 1984–1992. [[CrossRef](#)]
41. Papanikolaou, P.A.; Tkachenko, N.V. Probing the excited state dynamics of a new family of Cu(I)-complexes with an enhanced light absorption capacity: Excitation-wavelength dependent population of states through branching. *Phys. Chem. Chem. Phys.* **2013**, *15*, 13128–13136. [[CrossRef](#)] [[PubMed](#)]
42. Grupe, M.; Bappler, F.; Theiss, M.; Busch, J.M.; Dietrich, F.; Volz, D.; Gerhards, M.; Bräse, S.; Diller, R. Real-time observation of molecular flattening and intersystem crossing in [(DPEPhos)Cu(I)(PyrTet)] via ultrafast UV/Vis- and mid-IR spectroscopy on solution and solid samples. *Phys. Chem. Chem. Phys.* **2020**, *22*, 14187–14200. [[CrossRef](#)] [[PubMed](#)]
43. Iwamura, M.; Watanabe, H.; Ishii, K.; Takeuchi, S.; Tahara, T. Coherent Nuclear Dynamics in Ultrafast Photoinduced Structural Change of Bis(diimine)copper(I) Complex. *J. Am. Chem. Soc.* **2011**, *133*, 7728–7736. [[CrossRef](#)] [[PubMed](#)]
44. Capano, G.; Penfold, T.J.; Chergui, M.; Tavernelli, I. Photophysics of a copper phenanthroline elucidated by trajectory and wavepacket-based quantum dynamics: A synergetic approach. *Phys. Chem. Chem. Phys.* **2017**, *19*, 19590–19600. [[CrossRef](#)]
45. Capano, G.; Chergui, M.; Rothlisberger, U.; Tavernelli, I.; Penfold, T.J. A Quantum Dynamics Study of the Ultrafast Relaxation in a Prototypical Cu(I)-Phenanthroline. *J. Phys. Chem. A* **2014**, *118*, 9861–9869. [[CrossRef](#)]
46. Zgierski, M.Z. Cu(I)-2,9-dimethyl-1,10-phenanthroline: Density functional study of the structure, vibrational force-field, and excited electronic states. *J. Chem. Phys.* **2003**, *118*, 4045. [[CrossRef](#)]
47. Stoianov, A.; Gourlaouen, C.; Vela, S.; Daniel, C. Luminescent Dinuclear Copper(I) Complexes as Potential Thermally Activated Delayed Fluorescence (TADF) Emitters: A Theoretical Study. *J. Phys. Chem. A* **2018**, *122*, 1413–1421. [[CrossRef](#)]
48. Levi, G.; Biasin, E.; Dohn, A.O.; Jonsson, H. On the interplay of solvent and conformational effects in simulated excited-state dynamics of a copper phenanthroline photosensitizer. *Phys. Chem. Chem. Phys.* **2020**, *22*, 748–757. [[CrossRef](#)]
49. Du, L.; Lan, Z. Ultrafast structural flattening motion in photoinduced excited state dynamics of bis(diamine)copper(I) complex. *Phys. Chem. Chem. Phys.* **2016**, *18*, 7641–7650. [[CrossRef](#)]
50. Capano, G.; Rothlisberger, U.; Tavernelli, I.; Penfold, T.J. Theoretical Rationalization of the Emission Properties of Photophysical Cu(I)-phenanthroline Complexes. *J. Phys. Chem. A* **2015**, *119*, 7026–7037. [[CrossRef](#)]
51. Guda, A.; Windisch, J.; Probst, B.; van Bokhoven, J.A.; Alberto, R.; Nachtegaal, M.; Chen, L.X.; Smolentsev, G. Excited-State Structure of Copper Phenanthroline-Based Photosensitizers. *Phys. Chem. Chem. Phys.* **2021**, *23*, 26729–26736. [[CrossRef](#)] [[PubMed](#)]
52. Kalsani, V.; Schmittel, M.; Listorti, A.; Accorsi, G.; Armaroli, N. Novel Phenanthroline Ligands and Their Kinetically Locked Copper(I) Complexes with Unexpected Photophysical Properties. *Inorg. Chem.* **2006**, *45*, 2061–2067. [[CrossRef](#)] [[PubMed](#)]
53. Green, O.; Gandhi, B.A.; Burstyn, J.N. Photophysical Characteristics and Reactivity of Bis(2,9-di-tert-butyl-1,10-phenanthroline) Copper(I). *Inorg. Chem.* **2009**, *48*, 5704–5714. [[CrossRef](#)]
54. Garakyaraghi, S.; Koutnik, P.; Castellano, F.N. Photoinduced Structural Distortions and Singlet-Triplet Intersystem Crossing in Cu(I) MLCT Excited States Monitored by Optically Gated Fluorescence Spectroscopy. *Phys. Chem. Chem. Phys.* **2017**, *19*, 16662–16668. [[CrossRef](#)] [[PubMed](#)]
55. Garakyaraghi, S.; McCusker, C.E.; Khan, S.; Koutnik, P.; Bui, A.T.; Castellano, F.N. Enhancing the Visible-Light Absorption and Excited-State Properties of Cu(I) MLCT Excited States. *Inorg. Chem.* **2018**, *57*, 2296–2307. [[CrossRef](#)]
56. Brandl, T.; Kerzig, C.; Le Pleux, L.; Prescimone, A.; Wenger, O.S.; Mayor, M. Improved Photostability of a Cu^I Complex by Macrocyclization of the Phenanthroline Ligands. *Chem. Eur. J.* **2020**, *26*, 3119–3128. [[CrossRef](#)] [[PubMed](#)]
57. Livshits, M.Y.; Reeves, B.J.; DeWeerd, J.; Strauss, S.H.; Boltalina, O.V.; Rack, J.J. Trifluoromethylated Phenanthroline Ligands Reduce Excited-State Distortion in Homoleptic Copper(I) Complexes. *Inorg. Chem.* **2020**, *59*, 2781–2790. [[CrossRef](#)] [[PubMed](#)]
58. Rosko, M.C.; Wells, K.A.; Hauke, C.E.; Castellano, F.N. Next Generation Cuprous Phenanthroline MLCT Photosensitizer Featuring Cyclohexyl Substituents. *Inorg. Chem.* **2021**, *60*, 8394–8403. [[CrossRef](#)]
59. Frisch, M.J.; Trucks, G.W.; Schlegel, H.B.; Scuseria, G.E.; Robb, M.A.; Cheeseman, J.R.; Scalmani, G.; Barone, V.; Petersson, G.A.; Nakatsuji, H.; et al. *Gaussian 09*; Revision D.01; Gaussian, Inc.: Wallingford, CT, USA, 2016.
60. Becke, A.D. Density-functional thermochemistry. III. The role of exact exchange. *J. Chem. Phys.* **1993**, *98*, 5648–5652. [[CrossRef](#)]
61. Miertuš, S.; Scrocco, E.; Tomasi, J. Electrostatic interaction of a solute with a continuum. A direct utilisation of AB initio molecular potentials for the prevision of solvent effects. *Chem. Phys.* **1981**, *55*, 117–129. [[CrossRef](#)]
62. Ditchfield, R.; Hehre, W.J.; Pople, J.A. Self-consistent molecular-orbital methods. IX. An extended Gaussian-type basis for molecular-orbital studies of organic molecules. *J. Chem. Phys.* **1971**, *54*, 724. [[CrossRef](#)]

63. Grimme, S.; Antony, J.; Ehrlich, S.; Krieg, H. A consistent and accurate ab initio parametrization of density functional dispersion correction (DFT-D) for 94 elements H-Pu. *J. Chem. Phys.* **2010**, *132*, 154104. [CrossRef] [PubMed]
64. ADF, SCM, Theoretical Chemistry, Vrije Universiteit, Amsterdam, The Netherlands. Available online: <https://www.scm.com/doc/ADF/index.html> (accessed on 1 June 2019).
65. Van Lenthe, E.; Baerends, E.J. Optimized Slater-type basis sets for the elements 1–118. *J. Comp. Chem.* **2003**, *24*, 1142–1156. [CrossRef] [PubMed]
66. Van Lenthe, E.; van Leeuwen, R.; Baerends, E.J.; Snijders, J.G. Relativistic regular two-component Hamiltonians. *Int. J. Quant. Chem.* **1996**, *57*, 281–293. [CrossRef]
67. Grimme, S. Semiempirical GGA-Type Density Functional Constructed with a Long-Range Dispersion Correction. *J. Comput. Chem.* **2006**, *27*, 1787–1799. [CrossRef] [PubMed]
68. Klamt, A. Conductor-like Screening Model for Real Solvents: A New Approach to the Quantitative Calculation of Solvation Phenomena. *J. Phys. Chem.* **1995**, *99*, 2224–2235. [CrossRef]
69. Wang, F.; Ziegler, T. A simplified relativistic time-dependent density-functional theory formalism for the calculations of excitation, energies including spin-orbit coupling effect. *J. Chem. Phys.* **2005**, *123*, 154102–154112. [CrossRef] [PubMed]
70. Wang, F.; Ziegler, T.; van Lenthe, E.; van Gisbergen, S.; Baerends, E.J. The calculation of excitation energies based on the relativistic two-component zeroth-order regular approximation and time-dependent density-functional with full use of symmetry. *J. Chem. Phys.* **2005**, *122*, 204103–204112. [CrossRef]
71. Peach, M.J.G.; Tozer, D.J. Overcoming Low Orbital Overlap and Triplet Instability Problems in TDDFT. *J. Phys. Chem. A* **2012**, *116*, 9783–9789. [CrossRef]
72. Plasser, F. TheoDORE: A toolbox for a detailed and automated analysis of electronic excited state computations. *J. Chem. Phys.* **2020**, *152*, 084108. [CrossRef]
73. Wang, R.Z.; Xu, J.Q.; Yang, G.Y.; Bu, W.M.; Xing, Y.H.; Li, D.M.; Liu, S.Q.; Ye, L.; Fan, Y.G. Structure of [Cu(phen)₂]₂[(Cu(phen))₂Mo₈O₂₆].H₂O. *Pol. J. Chem.* **1999**, *73*, 1909.
74. Avdeeva, V.V.; Dziova, A.E.; Polyakova, I.N.; Malinina, E.A.; Goeva, L.V.; Kuznetsov, N.T. Copper(I), copper(II), and heterovalent copper(I,II) complexes with 1,10-phenanthroline and the closo-decaborate anion. *Inorg. Chim. Acta* **2015**, *430*, 74–81. [CrossRef]
75. Rheingold, A.L.; Department of Chemistry, University of California, La Jolla, CA, USA; Maatta, E.; Department of Chemistry, Kansas State University, Manhattan, KS, USA. CSD Communication, 2015.
76. Huang, Z.; Hartwig, J.F. Copper(I) Enolate complexes in α -Arylation Reactions: Synthesis, Reactivity and Mechanism. *Angew. Chem. Int. Ed.* **2012**, *51*, 1028–1032. [CrossRef] [PubMed]
77. Lin, X.; Hou, C.; Li, H.; Weng, Z. Decarboxylative Trifluoromethylating Reagent [Cu(O₂CCF₃)(phen)] and Difluorocarbene Precursor [Cu(phen)₂][O₂CCF₂Cl]. *Chem. Eur. J.* **2016**, *22*, 2075–2084. [CrossRef] [PubMed]
78. Hillhouse, G.; Searle Chemistry Laboratory, Department of Chemistry, The University of Chicago, Chicago, IL, USA; Rheingold, A.L.; Department of Chemistry, University of Delaware, Newark, DE, USA; Allen, M.B. CSD Communication, 1996.
79. Huang, Y.; Ajitha, M.J.; Huang, K.-W.; Zhang, Z.; Weng, Z. A class of effective decarboxylative perfluoroalkylating reagents: [(phen)₂Cu](O₂CRF). *Dalton Trans.* **2016**, *45*, 8468–8474. [CrossRef]
80. Yu, J.-H.; Lu, Z.-L.; Xu, J.-Q.; Bie, H.-Y.; Lu, J.; Zhang, X. Syntheses, characterization and optical properties of some copper(i) halides with 1,10-phenanthroline ligand. *New J. Chem.* **2004**, *28*, 940–945. [CrossRef]
81. Hamalainen, R.; Department of Inorganic Chemistry, University of Helsinki, Helsinki, Finland; Ahlgren, M.; Department of Inorganic Chemistry, University of Helsinki, Helsinki, Finland; Turpeinen, U.; Department of Inorganic Chemistry, University of Helsinki, Helsinki, Finland; Raikas, T.; Department of Inorganic Chemistry, University of Helsinki, Helsinki, Finland. Crystal Structure Communications, 1979.
82. Dessy, G.; Laboratorio di Teoria e Struttura Elettronica e Comportamento Spettrochimico dei Composti di Coordinazione del CNR, Monterotondo Stazione, Italy; Fares, V.; Laboratorio di Teoria e Struttura Elettronica e Comportamento Spettrochimico dei Composti di Coordinazione del CNR, Monterotondo Stazione, Italy. Crystal Structure Communications, 1979.
83. Royappa, A.T.; Royappa, A.D.; Moral, R.F.; Rheingold, A.L.; Papoular, R.J.; Blum, D.M.; Duong, T.Q.; Stepherson, J.R.; Vu, O.D.; Chen, B.; et al. Copper(I) oxalate complexes: Synthesis, structures and surprises. *Polyhedron* **2016**, *119*, 563–574. [CrossRef]
84. Zheng, S.-L.; Gembicky, M.; Messerschmidt, M.; Dominiak, P.M.; Coppens, P. Effect of the Environment on Molecular Properties: Synthesis, Structure, and Photoluminescence of Cu(I) Bis(2,9-dimethyl-1,10-phenanthroline) Nanoclusters in Eight Different Supramolecular Frameworks. *Inorg. Chem.* **2006**, *45*, 9281–9289. [CrossRef]
85. Kovalevsky, A.Y.; Gembicky, M.; Novozhilova, I.V.; Coppens, P. Solid-State Structure Dependence of the Molecular Distortion and Spectroscopic Properties of the Cu(I) Bis(2,9-dimethyl-1,10-phenanthroline) Ion. *Inorg. Chem.* **2003**, *42*, 8794–8802. [CrossRef] [PubMed]
86. Blake, A.J.; Hill, S.J.; Hubberstey, P.; Li, W.-S. Copper(I) chelated by 2,9-dimethyl-1,10-phenanthroline and bridged by 4,4'-bipyridine or trans-1,2-bis(pyridin-4-yl)ethene to give discrete dinuclear and polymeric cations. *J. Chem. Soc. Dalton Trans.* **1998**, 909–916. [CrossRef]
87. Gandhi, B.A.; Green, O.; Burstyn, J.N. Facile oxidation-based of sterically encumbered four-coordinate bis(2,9-di-*ter*-butyl-1,10-phenanthroline)copper(I) and related three-coordinate copper(I) complexes. *Inorg. Chem.* **2007**, *46*, 3816–3825. [CrossRef] [PubMed]

88. Asano, M.S.; Tomiduka, K.; Sekizawa, K.; Yamashita, K.; Sugiura, K. Temperature-dependent Emission of Copper(I) Phenanthroline Complexes with Bulky Substituents: Estimation of an Energy Gap between the Singlet and Triplet MLCT States. *Chem. Lett.* **2010**, *39*, 376–378. [[CrossRef](#)]
89. Czerwieniec, R.; Yersin, H. Diversity of Copper(I) Complexes Showing Thermally Activated Delayed Fluorescence: Basis Photophysical Analysis. *Inorg. Chem.* **2015**, *54*, 4322–4327. [[CrossRef](#)] [[PubMed](#)]
90. Farias, G.; Salla, C.A.M.; Heying, R.S.; Bortoluzzi, A.J.; Curcio, S.F.; Cazati, T.; dos Santos, P.L.; Monkman, A.P.; de Souza, B.; Bechtold, I.H. Reducing lifetime in Cu(I) Complexes with Thermally Activated Delayed Fluorescence and Phosphorescence Promoted by Chalcogenolate-diimine ligands. *J. Mater. Chem. C* **2020**, *8*, 14595–14604. [[CrossRef](#)]
91. Greenough, S.E.; Horbury, M.D.; Thompson, J.O.F.; Roberts, G.M.; Karsili, T.N.V.; Marchetti, B.; Townsend, D.; Stavros, V.G. Solvent induced conformer specific photochemistry of guaiacol. *Phys. Chem. Chem. Phys.* **2014**, *16*, 16187–16195. [[CrossRef](#)]
92. Miller, M.T.; Gantzel, P.K.; Karpishin, T.B. Structures of the Copper(I) and Copper(II) Complexes of 2,9-Diphenyl-1,10-phenanthroline: Implications for Excited-State Structural Distortion. *Inorg. Chem.* **1998**, *37*, 2285–2290. [[CrossRef](#)]
93. Gimeno, L.; Blart, E.; Rebilly, J.-N.; Coupeau, M.; Allain, M.; Roisnel, T.; Quarré de Verneuil, A.; Gourlaouen, C.; Daniel, C.; Pellegrin, Y. Non-symmetrical sterically challenged phenanthroline ligands and their homoleptic copper(I) complexes with improved excited state properties. *Chem. Eur. J.* **2020**, *26*, 11887–11899. [[CrossRef](#)] [[PubMed](#)]
94. Heuft, M.A.; Fallis, A.G. Template-directed synthesis of helical phenanthroline cyclophanes. *Angew. Chem. Int. Ed.* **2002**, *41*, 4520–4523. [[CrossRef](#)]
95. Dietrich-Buchecker, C.O.; Guilhem, J.; Khemiss, A.K.; Kintzinger, J.-P.; Pascard, C.; Sauvage, J.-P. Molecular Structure of a [3]Catenate: Curling Up of the Interlocked System by Interaction between the Two Copper Complex Subunits. *Angew. Chem. Int. Ed. Engl.* **1987**, *26*, 661–663. [[CrossRef](#)]
96. Gimeno, L.; Phelan, B.T.; Sprague-Klein, E.A.; Roisnel, T.; Blart, E.; Gourlaouen, C.; Chen, L.X.; Pellegrin, Y. Bulky and Stable Copper(I)-Phenanthroline Complex: Impact of Steric Strain and Symmetry on the Excited-State Properties. *Inorg. Chem.* **2022**, *61*, 7296–7307. [[CrossRef](#)]